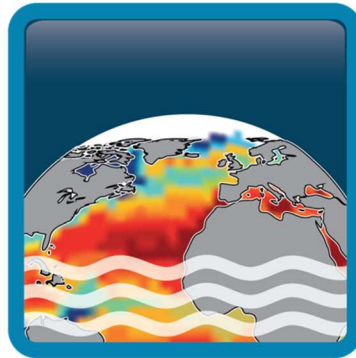


Climate Change Initiative+ (CCI+) Phase 2

Sea Surface Salinity



[D4.1] Product Validation and Intercomparison Report (PVIR)

Customer: ESA

Ref.: ESA-EOP-SC-AMT-2021-26

Version: v5.1

Ref. internal: 4000123663/18/I-NB

Revision Date: 25/02/2025



Signatures

Authors	Adrien Martin	NOC/NOVELTIS	
	Sébastien Guimbard	OceanScope	
	Nicolas Kolodziejczyk	LOPS	
Reviewed By	Chris Banks	NOC	
Approved By	Jacqueline Boutin (Science Leader)	LOCEAN	
	Nicolas Reul (Science Leader)	IFREMER	
	Rafael Catany (Project Manager)	ARGANS	
Accepted By	Roberto Sabia (Technical Officer)	ESA	

Diffusion List

Sea Surface Salinity Team Members

Amendment Record Sheet

Date / Issue	Description	Section / Page
	For previous amendment record sheet, please consult v3	
21/01/2024	Delivery to ESA for version 4	New document
20/12/2024	Delivery to ESA for version 5	Update figures, tables and descriptions with results obtained with version 5 + addition of an appendix for C-band products
25/02/2025	Revision 1 of version 5	Correction of typos

Table of Contents

1	Introduction	1
1.1	Scope of this document	1
1.2	Structure of the document	1
1.3	Applicable Documents.....	1
1.4	Reference Documents	1
2	Executive Summary	3
2.1	Sea Surface Salinity products	3
2.2	Main results	3
2.3	Main results from Pi-MEP match-up reports.....	4
2.4	D.....	4
3	Validation: Data & Methods	5
3.1	Fiducial Reference Measurements	5
3.1.1	Level of independence to CCI products.....	5
3.2	In situ Dataset.....	6
3.2.1	Argo match-ups database: Pi-MEP MDB.....	6
3.2.2	Reference Dataset: Gridded MDB	7
3.3	Uncertainty validation	7
3.4	Quality metrics.....	9
4	Validation of Products, Stability, Resolution and Product Uncertainty Estimates	10
4.1	Accuracy & Precision	10
4.1.1	Global products validation for L4	10
4.1.2	Arctic Case Study	15
4.2	Time series stability: intra-annual & long-term stability.....	18
4.3	In Situ Vertical Representiveness Error.....	21
4.4	Temporal & spatial effective resolution	22
4.4.1	Temporal effective resolution	22
4.4.2	Spatial effective resolution: Assessment of mesoscale features in Tropical Atlantic	24
4.5	Uncertainty.....	28
4.5.1	Normalised SSS.....	28
4.5.2	Compared SSS Distribution	29
4.5.3	Estimation of mismatch error using GLORYS 1/12°	30
Annex A	Validation of C/X-band CCI Products.....	34
A1.	Amazon-Orinoco river plumes	34
A2.	Niger-Congo river plumes	36
A3.	Mississippi river plumes	37

A4.	Bay of Bengal	39
------------	----------------------------	-----------

List of figures

Figure 4-1: (top-left) L4 CCIv5 monthly SSS for the 15th of January 2015, (top-right) Argo salinity measurements from the Pi-MEP MDB for the same month. (middle/bottom-left) temporal median/robust standard deviation of L4 CCIv5 SSS and (middle/bottom-right) temporal median/robust standard deviation of the gridded MDB SSS. Diagonal hatching indicates regions with less than 30 points over the full time-series.----- 11

Figure 4-2: temporal median for Antarctic (top) and Arctic (bottom), of (right) Argo gridded MDB SSS and (left) L4 CCIv5 SSS. Diagonal hatching indicates regions with less than 30 points over the full time-series. ----- 12

Figure 4-3: Histogram of all pairwise gridded MDB (left) Argo SSS in grey and CCI L4 v5 SSS in green; (right) Gridded MDB of the CCI L4 v5 minus Argo difference, (blue line) normalized probability function (PDF) using computed mean and standard deviation, (orange curve) normalized PDF using computed median and robust standard deviation. ----- 12

Figure 4-4 (top-left) Temporal median and (top-right) temporal robust standard deviation of gridded pairwise SSS differences between CCI and Argo. (on the left) A moving window of 2 pixels in longitude and latitude is applied to the median in order to highlight statistical significance (at 95%) which are indicated with dots. (on the right) Robust standard deviation calculated with less than 30 valid grid points in time are hatched. (bottom) differences of the temporal median differences between CCI and Argo between version 5 and version 4 using the comparison dataset.----- 14

Figure 4-5 (top) SSS difference between CCI+SSSv5.5 Arctic product and ICES in situ measurements between 2010-2022 in the Barents Sea; (middle) Scatter plot between CCI+SSSv5.5 and in situ measurements; (bottom) SSS difference as a function of the in situ SST (in °C).----- 17

Figure 4-6: (1st panel): mean SSS of gridded MDB of pairwise Argo in red and L4 CCI in black for v5 and in orange and green for comparison v4 and v5; (2nd panel) Average of; (3rd panel) standard deviation of; the gridded MDB of the pairwise SSS difference between CCI and Argo. Solid lines represent (2nd panel) the median (3rd panel) the robust standard deviation. Dashed lines represent (2nd panel) the mean (3rd panel) the standard deviation. The shading indicates the 95% confidence interval. (4th panel) number of valid gridded MDB values. ----- 18

Figure 4-7: Global latitude-time Hovmöller of the gridded MDB of the pairwise CCI difference with Argo for L4 v5. Each pixel represents the median value after a moving window over 2 pixels in latitude and time. Data which are significantly different from 0 (at 95%) are indicated with dots. All sub-figures share the same colour bar. ----- 19

Figure 4-8: Global latitude-time Hovmöller of the gridded MDB of the pairwise CCI difference with Argo for (top) L4 v4 comparison dataset; (middle) L4 v5 comparison dataset; (bottom) Absolute difference between the two subplots above. Green indicates improvement towards zero; Red indicates degradation away from zero. Each pixel represents the median value after a moving window over 2 pixels in latitude and time. Data which are significantly different from 0 (at 95%) are indicated with dots. All sub-figures share the same colour bar. ----- 20

Figure 4-9: Seasonal climatology of the gridded pairwise CCI L4 difference with Argo calculated using the median. A moving window average of 2 x 2 pixels in longitude and latitude have been

applied to increase the number of sampled, hence the significativity. Pixels, which are statistically significant (at 95%) are indicated with dots.-----	21
Figure 4-10: Seasonal Salinity gradient (in pss/m) derived from Argo at 5 m and 10 m. Gradient are gridded on the same grid as used for the pairwise difference (bi-weekly; 175 km). -----	22
Figure 4-11 : Average power spectrum of SSS from (black) moorings, (red) CCI Weekly products, (blue) ISAS, (pink) Mercator; (top) for CCI L4 Weekly v4.4; (bottom) for CCI L4 Weekly v5.5. from Pi-MEP. -----	23
Figure 4-12: Average power spectrum of SSS from (black) moorings, (red) CCI Monthly products, (blue) ISAS, (pink) Mercator; (top) for CCI L4 Weekly v4.4; (bottom) for CCI L4 Weekly v5.5. from Pi-MEP. -----	24
Figure 4-13: CCI+SSS on 30 June 2011 with (dashed line) 92 TSG transects in the Subtropical North Atlantic) and (solid line) 27 TSG transect in the Tropical Atlantic. All SSS transects have been carried out between 2011-2016. -----	25
Figure 4-14: a) Density spectra from from 92 collocated TSG (black); CCI+SSS v5 (solid red) SSS transects in Subtropical North Atlantic. Vertical thick black bar is the level of confidence at 95%. b) Coherency between the TSG and CCI+SSS SSS transects. Dashed line is the level of significance at 95%. c) Density spectra from from 27 collocated TSG (black)/CCI+SSS(red) SSS transects in Tropical Atlantic. Vertical thick black bar is the level of confidence at 95%. d) Coherency between the TSG and CCI +SSS SSS transects. Dashed line is the level of significance at 95%. -----	27
Figure 4-15 : Time series of the normalised SSS normalised using (A) the satellite uncertainty; (B) the total uncertainty combining the satellite and reference uncertainty. Top row for each panel represents (solid line) the median and (dashed line) the mean. Bottom row for each panel represents (solid line) the robust standard deviation and (dashed line) the classic standard deviation. Colours are for the L4v5 and the comparison dataset for L4v4 and L4v5. -----	29
Figure 4-16: measured standard deviation (green and red dots) for classic and robust standard deviation respectively; of the gridded pairwise CCI/Argo difference (dSSS) for each uncertainty 0.05 bin. (top) using satellite uncertainty; (bottom) using total uncertainty - satellite + reference (column from left to right) for comparison dataset L4v5 and comparison dataset L4v4. The size of the circle indicates the number of data. -----	30
Figure 4-17: (top) Temporal median and (bottom) temporal robust standard deviation of the estimated sampling mismatch using GLORYS. This sampling mismatch estimates is obtained from the difference between GLORYS averaged over 50km, 30 days and GLORYS sampled at Argo time and position (horizontal and vertical). The colour scale is zoomed by 40% compared to the colour scale in Figure 4-4. -----	31
Figure 4-18: (top) mean and (bottom) standard deviation of the observed difference between CCI and Argo per bins of expected mismatch using GLORYS with the different resampling strategy represented in colour (see legend). For clarity, on the top figure, only the most significant plots are presented. -----	32
Figure A 1: Pairwise comparison between CCI C/X-band and in situ measurements from (left) EN4 and (right) CORA datasets-----	34

Figure A 2: Pairwise comparison between CCI C/X-band and in situ measurements on a 1°x1° grid and showing (left) the mean difference and (right) the RMSD. ----- 35

Figure A 3: Time series of the RMSD against EN4 over the Bay of Bengal for the full time series including the C/X-band and L-band period. ----- 35

Figure A 4: Pairwise comparison between CCI C/X-band and in situ measurements from EN4 dataset. ----- 36

Figure A 5: Pairwise comparison between CCI C/X-band and in situ measurements on a 1°x1° grid and showing (left) the mean difference and (right) the RMSD. ----- 36

Figure A 6: Time series of the RMSD against EN4 over the Bay of Bengal for the full time series including the C/X-band and L-band period. ----- 37

Figure A 7: Pairwise comparison between CCI C/X-band and in situ measurements from (left) EN4 and (right) CORA datasets----- 37

Figure A 8: Pairwise comparison between CCI C/X-band and in situ measurements on a 1°x1° grid and showing (left) the mean difference and (right) the RMSD. ----- 38

Figure A 9: Time series of the RMSD against EN4 over the Bay of Bengal for the full time serie including the C/X-band and L-band period. ----- 38

Figure A 10: Pairwise comparison between CCI C/X-band and in situ measurements from (left) EN4 and (right) CORA datasets----- 39

Figure A 11: Pairwise comparison between CCI C/X-band and in situ measurements on a 1°x1° grid and showing (left) the mean difference and (right) the RMSD. ----- 40

Figure A 12: Time series of the RMSD against EN4 over the Bay of Bengal for the full time serie including the C/X-band and L-band period. ----- 40

List of tables

Table 1 Applicable documents (as seen in CCI+SSS website, http://cci.esa.int/salinity)-----	1
Table 2 Reference documents -----	1
Table 3: Statistics for Pi-MEP MDB comparison dataset for v4 and v5 using exactly the same Argo floats collocation. Cf Pi-MEP reports for the details about the conditions criteria. -----	13
Table 4: Statistics of CCI L4 v5.5 30dr against in situ data for the global ocean applying criteria C1 (only pairs where RR=0 mm/h, $3 < U < 12$ m/s, SST > 5°C, distance to coast > 800 km). From Pi-MEP -----	15

Acronyms (Check from SOW)

AD	Applicable document
ADB	Actions database
AMOC	Atlantic Meridional Overturning Circulation
ATBD	Algorithm theoretical basis documents
BRO	Brochure
CLIC	Climate and Cryosphere
DIR	Directory
DS	Dataset availability
DS-UM	Dataset user manual
DVP	Development and validation plan
EC RTD	European Commission Directorate General for Research and Innovation
EDS	Experimental dataset
EMI	Electromagnetic Interference
EO	Earth Observation
EOEP	Earth Observation Envelope Program
ESA	European Space Agency
FR	Final review
FWF	Freshwater fluxes
GCOS	Global Climate Observing System
IAR	Impact assessment report
ITT	Invitation to tender
IPP	Year of Polar Prediction
KO	Kick-off
MR	Monthly report
MTR	Mid-term review
MV-TN	Modelling and validation technical note
NDVI	Normalized Difference Vegetation Index
PAR	Preliminary analysis report
PGICs	Peripheral glaciers and ice caps
PM	Progress meeting
PMP	Project management plan
RD	Reference document
RB	Requirements baseline
SAR	Synthetic Aperture Radar
SIAR	Scientific and impact assessment report
SMOS	Soil Moisture and Ocean Salinity
SoW	Statement of work
SR	Scientific roadmap
SSS	Sea Surface Salinity

SST	Sea Surface Temperature
TDP	Technical data package
TDS	Training Data Set
TN	Technical note
VIR	Validation and intercomparison report
VR	Validation report
WCRP	World Climate Research Programme
WP	Work package
WS	Workshop minutes
WWRP	World Weather Research Programme
AD	Applicable document
ADB	Actions database
AMOC	Atlantic Meridional Overturning Circulation
ATBD	Algorithm theoretical basis documents
BRO	Brochure
CLiC	Climate and Cryosphere
DIR	Directory
DS	Dataset availability
DS-UM	Dataset user manual
DVP	Development and validation plan
EC RTD	European Commission Directorate General for Research and Innovation
EDS	Experimental dataset
EMI	Electromagnetic Interference
EO	Earth Observation
EOEP	Earth Observation Envelope Program
ESA	European Space Agency
FR	Final review
FWF	Freshwater fluxes
GCOS	Global Climate Observing System
IAR	Impact assessment report
ITT	Invitation to tender
IPP	Year of Polar Prediction
KO	Kick-off
MR	Monthly report
MTR	Mid-term review
MV-TN	Modelling and validation technical note
NDVI	Normalized Difference Vegetation Index
PAR	Preliminary analysis report



1 Introduction

1.1 Scope of this document

This document holds the Product Validation and Intercomparison Report (PVIR) prepared by the CCI+SSS team, as part of the activities included in WP400 of the Proposal (Task 4 from SoW ref. ESA-EOP-SC-AMT-2021-26).

This report contains an assessment of the L-band CCI version 5 products for Level 4 products for weekly and monthly time periods. The products are based on a temporal optimal interpolation of SSS data measured by SMOS, Aquarius-SAC and SMAP satellite missions.

This report also contains a validation of the C/X-band products obtained from AMSR-E over tropical river plumes.

1.2 Structure of the document

This document is composed of four sections:

Section 1 introduces the purpose and scope of the document. Section 2 provides an executive summary of the results presented. Section 3 presents the data and methods used for the systematic validation presented in Section 4. In Annex A, there is validation of the C/X-band products over tropical river plumes.

1.3 Applicable Documents

Table 1 Applicable documents (as seen in CCI+SSS website, <http://cci.esa.int/salinity>)

PSD	Product Specification Document	SSS_cci_PHASE#02-D1.2-PSD-v3.0
PUG	Product User Guide	SSS_cci_PHASE#02-D4.3-PUG-v4.0
PVP	Product Validation Plan	SSS_cci_PHASE#02-D2.5-PVP-v2.0
SoW	CCI+ Statement of Work	SOW

1.4 Reference Documents

Table 2 Reference documents

ID	Document	Reference
RD01	Product Validation Plan	SSS_cci_PHASE#02-D2.5-PVP-v2.0
RD02	In-situ database Analyses Report. Pi-MEP consortium. June 2023; Match-up database Analyses report, CCI L4 ESA GLOBAL MERGED-OI V4.4-MONTHLY Argo Global Ocean: pimep-mdb-report_GO_cci-l4-esa-merged-oi-v4.4-30dr_argo_20230615.pdf	



ID	Document	Reference
RD03	Guimbard, S.; Reul, N.; Sabia, R.; Herlédan, S.; Khoury Hanna, Z.E.; Piollé, J.-F.; Paul, F.; Lee, T.; Schanze, J.J.; Bingham, F.M.; Le Vine, D.; Vinogradova-Shiffer, N.; Mecklenburg, S.; Scipal, K.; Laur, H. The Salinity Pilot-Mission Exploitation Platform (Pi-MEP): A Hub for Validation and Exploitation of Satellite Sea Surface Salinity Data. <i>Remote Sens.</i> 2021 , <i>13</i> , 4600. https://doi.org/10.3390/rs13224600	
RD03	G. Reverdin, S. Morisset, L. Marié, D. Bourras, G. Sutherland, B. Ward, J. Salvador, J. Font, Y. Cuyper, L.R. Centurioni, V. Hormann, N. Koldziejczyk, J. Boutin, F. D'Ovidio, F. Nencioli, N. Martin, D. Diverres, G. Alory & R. Lumpkin (2015). Surface salinity in the North Atlantic subtropical gyre during the STRASSE/SPURS summer 2012 cruise. <i>Oceanography</i> 28 (1): 114-123	
RD04	N. Hoareau, A. Turiel, M. Portabella, J. Ballabrera-Poy & J. Vogelzang (2018). Singularity Power Spectra: A Method to Assess Geophysical Consistency of Gridded Products - Application to Sea-Surface Salinity Remote Sensing Maps. <i>IEEE Transactions on Geosciences and Remote Sensing</i> 56, 5525-5536	Hoareau et al., 2018
RD05	ATBD	SSS_cci_PHASE#02_D2.3-ATBD-v4.0
RD06	End-to-End ECV Uncertainty Budget - E3UB	SSS_cci_PHASE#02_D2.3-E3UB-v4.0
RD07	Product Validation Plan version #1	SSS_cci-D2.5-PVP-v1.1
RD08	GLORYS 1/12° Reanalysis	
RD09	Product Validation and Intercomparison Report version 4	
	Stammer et al., 2020, How good do we know ocean salinity and its changes? <i>Progress in Oceanography</i> , vol. 190, p. 102478, 2021, doi: https://doi.org/10.1016/j.pocean.2020.102478	Stammer et al., 2020
	Boutin et al 2016, Satellite and In Situ Salinity: Understanding Near-surface Stratification and Sub-footprint Variability, <i>Bulletin of American Meteorological Society</i> , 97(10), doi: 10.1175/BAMS-D-15-00032.1	Boutin et al 2016
	Supply, A., J. Boutin, J.-L. Vergely, N. Kolodziejczyk, G. Reverdin, N. Reul, and A. Tarasenko (2020), New insights into SMOS sea surface salinity retrievals in the Arctic Ocean, <i>Remote Sensing of Environment</i> , 249, 112027, https://doi.org/10.1016/j.rse.2020.112027 .	Supply et al, 2020a
	Supply, A., J. Boutin, G. Reverdin, J.-L. Vergely, and H. Bellenger, 2020: Variability of satellite sea surface salinity under rainfall. In: <i>Satellite Precipitation Measurement</i> , V. Levizzani, C. Kidd., D. B. Kirschbaum, C. D. Kummerow, K. Nakamura, F. J. Turk, Eds., Springer Nature, Cham, <i>Advances in Global Change Research</i> , 69, 1155-1176, https://doi.org/10.1007/978-3-030-35798-6_34 .	Supply et al, 2020b
	Supply, A., Boutin, J., Kolodziejczyk, N., Reverdin, G., Lique, C., Vergely, J.-L., & Perrot, X. (2022). Meltwater lenses over the Chukchi and the Beaufort seas during summer 2019: From in situ to synoptic view. <i>Journal of Geophysical Research: Oceans</i> , 127, e2021JC018388. https://doi.org/10.1029/2021JC018388	Supply et al., 2022
	Hudson, P. A., Martin, A., Josey, S., Marzocchi, A., and Angeloudis, A.: Drivers of Laptev Sea interannual variability in salinity and temperature, <i>EGU sphere [preprint]</i> , https://doi.org/10.5194/egusphere-2023-1403 , 2023.	Hudson et al., 2023



2 Executive Summary

2.1 Sea Surface Salinity products

The products validated are:

CCI Level 4 version 5 products (referred in the following either as v5.5 or v54) for Weekly and Monthly averaged products. The products are distributed in three grids:

Using a regular 0.25° grid for the global ocean:

```
ESACCI-SEASURFACESALINITY-L4-SSS-GLOBAL-  
MERGED_OI_7DAY_RUNNINGMEAN_DAILY_0.25deg-xxxxxxx-fv5.5.nc  
ESACCI-SEASURFACESALINITY-L4-SSS-GLOBAL-  
MERGED_OI_Monthly_CENTRED_15Day_0.25deg-xxxxxxx-fv5.5.nc
```

Using an equal area (EASE2) grid for the Northern and Southern poles:

Northern Hemisphere

```
ESACCI-SEASURFACESALINITY-L4-SSS-POLAR-  
MERGED_OI_7DAY_RUNNINGMEAN_DAILY_25kmEASE2-NH-xxxxxxx-fv5.5.nc  
ESACCI-SEASURFACESALINITY-L4-SSS-POLAR-  
MERGED_OI_Monthly_CENTRED_15Day_25kmEASE2-NH-xxxxxxx-fv5.5.nc
```

Southern Hemisphere

```
ESACCI-SEASURFACESALINITY-L4-SSS-POLAR-  
MERGED_OI_7DAY_RUNNINGMEAN_DAILY_25kmEASE2-SH-xxxxxxx-fv5.5.nc  
ESACCI-SEASURFACESALINITY-L4-SSS-POLAR-  
MERGED_OI_Monthly_CENTRED_15Day_25kmEASE2-SH-xxxxxxx-fv5.5.nc
```

Full description of the dataset can be found in the Product User Guide (PUG). The products follow recommendations of the Product Specification Document (PSD).

2.2 Main results

- In situ reference dataset derived from Argo floats upper salinity measurements (see details in section 3.1 below);
- No systematic biases against reference data found (see details in summary for Pi-MEP match-up report in section 2.3 below for more details);
- Global precision against reference gridded data is of 0.14;
- CCI version 5 products show better performance than version 4, in particular the systematic underestimation in 2010 and the issue linked to SMAP between April to August have been resolved;
- Remaining seasonal oscillation of CCI SSS differences against reference:
 - Amplitude is maximum in the Northern Hemisphere (particularly > 40°N);
- Mesoscale features in Tropical Atlantic are coherent between CCI v5 and TSG transects up to a wavelength of 250-300km (features of ~150km);



- Uncertainties provided in CCI product are in good agreement with observations (within 30%).

2.3 Main results from Pi-MEP match-up reports

- No global bias found against Argo except for filtered collocations where:
 - SSS less than 33 pss (CCI saltier by 0.06 pss);
 - SSS higher than 37 pss (CCI fresher by 0.04 pss);
- Global precision (robust standard deviation; pairwise difference) against Argo of 0.15 pss
 - Decreasing to 0.12 and 0.13 pss for optimal region (>800 km from the coast);
 - Increasing to 0.2 pss for area characterised by one of the following conditions: rain and low wind; area with temporal standard deviation >0.2 pss; within 150 km of the coast; or SSS < 33 pss;
- The systematic global underestimation of 0.1 pss of SSS starting at the beginning of the dataset for about one year has been resolved for v5.
- Compared to Argo, similar performance for v4 and v5, with improvements for v5 close to the coast (< 150 km) and for high salinity values (> 37 pss), but slight degradation for low SST (< 5°C) as sampled by Argo.
- Reduction of systematic biases in the Arctic against various in situ platforms for v5 compared to v4.
- Good agreement between the observed CCI SSS product temporal power spectra and moorings for the two-averaging period (weekly and monthly).

2.4 D

CAVEATS

- There is a seasonal varying bias (< 0.05 pss) in the Northern Hemisphere.



3 Validation: Data & Methods

This section describes the Data and Methods used for the main validation results given in section 4.

3.1 Fiducial Reference Measurements

According to the GEO/CEOS Quality Assurance for Earth Observation (QA4EO), Fiducial Reference Measurements (FRM) are a suite of independent, fully characterized, and traceable ground measurements for the validation of satellite SSS. FRM must be characterised (and documented) for the property for which they are a reference; at a level commensurate with the application; temporally stable over the period of use; a value must be SI traceable or community agreed; and must be accompanied by a procedure on use.

In this report, all validation datasets are provided and documented by Pi-MEP [RD03] using community standards with quality control checks. In the following subsection we will define the level of independence against the CCI products.

3.1.1 Level of independence to CCI products

CCI L4v5 products are a combination of SMOS, Aquarius and SMAP products. Each product is adjusted to a base dataset to correct for unresolved bias. This section summarises the various adjustments to that base, to define these bases and their underlying *in situ* dataset. For further details, please refer to the ATBD [RD05] and E3UB [RD06].

CCI L4v5 products are adjusted pixel-by-pixel to get the same quantile over the full-time series (~12 years) than the quantile (typically 50% for the median, but in river plumes it goes to 80%, see [RD05] for details) of a base. South of 65°N, the base is defined as a combination of ISAS 2017 (for the period 2011-2017) and ISAS NRT (for the period 2018 to December 2023). Due to issues in climatology used as prior in these ISAS fields in the Arctic Ocean, north of 70°N, the pixel-by-pixel adjustment is derived from the median of CCI L4 climatological fields (after ice filtering) and a new *in situ* derived climatology. A cosine transition function is applied between 65°N and 70°N. Adjustments are excluded for the 1st year (in 2010, due to bias in SMOS data at the beginning). There is an additional latitudinal adjustment to correct for seasonal biases based on the same base.

The temporal median over the full period of the base is taken as the prior for the objective analysis used to produce the L4.

The main base used for calibration has the following differences:

- ISAS 2017: contains the following *in situ* datasets: Argo, CTD (ICES, CCHDO), moorings. It does not contain TSG or drifters.
- ISAS NRT: contains all observations included in Coriolis including TSG and drifters.

These corrections do not influence the interannual or longitudinal variability of the product.



3.2 In situ Dataset

Following PVP [RD1] recommendations, the reference dataset used for product validation is based on:

- *In situ* measurements of close-to-surface (<10 m) Argo from Pi-MEP

The reasoning for this choice of reference dataset is as follows:

- In the list of acceptable Fiducial Reference Measurements (FRM) referred to in PVP [RD1], the Argo dataset has been selected as it is the only dataset to provide regularly an almost complete coverage of global open water ocean. The temporal distribution from 2010 is also homogeneous [Pi-MEP – RD2].

In the following, the Argo dataset is described with its collocation criteria along with the gridding method and the method to estimate representativeness errors and validate uncertainties. A summary of the spatial (horizontal) representativeness error of *in situ* measurement, as described in the PVP [RD1], is given here. Finally, quality metrics to assess CCI products are presented.

The weekly products use monthly fields on which observed variability is added, therefore the focus of this summary report is on monthly fields, unless mentioned otherwise. We report in this document on validation against other *in situ* dataset (TSG, drifters, measurements using mammals) which are provided from Pi-MEP. A description of these datasets and full validation of Weekly and Monthly fields are available from:

- <https://pimep.ifremer.fr/diffusion/analysis/>
- <ftp://ftp.ifremer.fr/ifremer/cersat/pimep/diffusion/analysis/>

3.2.1 Argo match-ups database: Pi-MEP MDB

The Argo floats used for validation have been taken from Pi-MEP [RD02, RD03] where quality control checks have already been completed. The text below is an extract of the detailed description of the Argo dataset and of the collocation (Match-ups Data Base - MDB) with CCI+SSS products.

Argo is a global array of ~3,000 free-drifting profiling floats that measure oceanic variables including temperature and salinity of the upper 2000 m. This allows continuous monitoring of the temperature and salinity of the upper ocean, with all data being relayed and made publicly available within hours of collection. The array provides around 100,000 temperature and salinity profiles per year distributed over the global open water oceans at an average of 3-degree spacing. These data were collected and made freely available by the international Argo project and the national programs that contribute to it [Argo (2000)]. Only Argo salinity and temperature float data with a quality index set to 1 or 2 and data mode set to real time (RT), real time adjusted (RTA) or delayed mode (DM) are included in Pi-MEP. All measurements from Argo floats that may have problems with one or more sensors and appear in the grey list maintained at the Coriolis/GDACs are discarded. Furthermore, Pi-MEP provides an additional list of ~1000 "suspicious" Argo salinity profiles that are also removed before analysis. The upper ocean salinity and temperature values recorded between 0 m and 10 m depth are considered as Argo sea surface salinities (SSS) and sea surface temperatures (SST).

	Climate Change Initiative+ (CCI+) Phase 2	Ref.: ESA-EOP-SC-AMT-2021-26 Date: 25/02/2025 Version : v5.1 Page: 7 of 55
--	--	---

The Argo MDB is produced from the previously described cleaned quality controlled Pi-MEP Argo dataset. For the monthly CCI+SSS product, the match-up temporal window radius is 7.5 days around the central date of each satellite time step (bi-weekly, monthly averaged). The spatial window is 12.5 km radius for each node at the centre of the 25 km grid. If more than one satellite pixel meets these criteria then the final satellite SSS match-up point is the closest in time from the *in situ* measurement. The spatial and temporal offsets between the *in situ* and satellite data are stored in the MDB files alongside a wide range of colocalised auxiliary information.

There are three separate Argo MDB products from Pi-MEP:

- the baseline MDB covering the full CCI L4v5 time series;
- two MDB specific for the comparison between CCI L4v4 and CCI L4v5. For these two MDBs, only Argo floats collocated with both CCI v4 and v5 products are used. Given CCI v4 stops in 2022, it is per construction the case for these two MDBs.

All the data are freely available as NetCDF files at:

- <https://pimep.ifremer.fr/diffusion/data/>
- <ftp://ftp.ifremer.fr/ifremer/cersat/pimep/diffusion/data/>

The baseline MDB is used as it is in all Pi-MEP reports, and it will be specified in the text if the context is different from that described in §3.2.2 below.

3.2.2 Reference Dataset: Gridded MDB

Typically, Argo floats sample the water column every 10 days. In order to study some specific processes with strong temporal variability, some Argo floats profile the water column up to every 2 hours. The floats tend to be located in areas where SSS variability is strong and artificially increase the number of collocations in these specific areas. Consequently, it degrades comparisons against satellite based SSS. To solve this issue, following PVP [RD01-section 3.3.5] recommendations, a Monte Carlo approach is used. A sample is randomly selected from each grid cell (biweekly; 25km Equal Area EASE2 grid) and is repeated a multiple number of times (here nine times). All validation metrics are computed for each subsample (e.g. difference satellite and *in situ*). The multiple subsamples are aggregated together by calculating the median. The spatial sampling is subsampled by a factor of seven in both latitude and longitude to ensure sufficient data for a given pixel over the full time series and get significative statistics. Each grid point corresponds to a 175 km Equal Area EASE grid.

This approach is applied for the baseline MDB covering the full CCI L4 v5 time series for gridded MDB and is used as the reference and is referred simply as “v5.5” or “v5” for short. The same method is applied for the two MDB specific for the comparison between CCI L4v4 and L4v5. They are referred respectively as “compv4” and “compv5”.

3.3 Uncertainty validation

To validate satellite uncertainty estimates, the approach is to compare the distribution of the difference of satellite SSS minus reference SSS ($\Delta SSS = CCI - ref$). In an ideal scenario, the ΔSSS temporal standard deviation equals the pixel-based satellite uncertainty ($\Delta\sigma_{sat}$):



$$\sigma_{\Delta SSS=CCI-re} = \Delta\sigma_{sat}$$

However, as stated in the PVP [RD1] the geophysical variability of reference SSS data over the time-space scale of remote sensing products depends not only on the particular spatial resolution and time window defining the remote sensing products, but also on the region at which this variability is estimated (inter-regional variability being quite significant [RD3]). Consequently, the ΔSSS standard deviation is a combination of both the satellite SSS uncertainty and the uncertainty in the reference SSS ($\Delta\sigma_{ref}$):

$$\sigma_{\Delta SSS} = \sqrt{\Delta\sigma_{sat}^2 + \Delta\sigma_{ref}^2}$$

In the reference uncertainty all the following terms are included:

- $\Delta\sigma_{meas.}$: Measurement uncertainty (direct ground-truth instrument error);
- $\Delta\sigma_{space}$: Spatial representativeness error (difference in spatial sampling of a point measurement versus a surface measurement defined by a grid cell);
- $\Delta\sigma_{time}$: Time representativeness error;
- $\Delta\sigma_{vertical}$: Vertical representativeness error (difference in depth of the measurements).

The reference uncertainty corresponds to the following combination assuming gaussian distribution and independent errors:

$$\Delta\sigma_{ref} = \sqrt{\Delta\sigma_{space}^2 + \Delta\sigma_{time}^2 + \Delta\sigma_{vertical}^2 + \Delta\sigma_{meas.}^2}$$

In the following, we assume the measurement uncertainty to be negligible ($\Delta\sigma_{meas.} = 0$). This is true at first order as we consider all poor measurements to have been discarded with the quality control and filtering methods applied by Pi-MEP.

In section 4.5.3, we estimate the full representativeness error (aka mismatch error) in space (horizontal and vertical) and time using the 1/12° daily GLORYS numerical reanalysis [RD08].

The vertical representativeness error from Argo floats measurements is discussed in section 4.3.

In section 4.5.1 and 4.5.2, the vertical representativeness error is neglected ($\Delta\sigma_{vertical} = 0$). The time representativeness error, although sometimes important (e.g. river plumes), is not considered ($\Delta\sigma_{time} = 0$). Argo measurements have been selected in a +-7.5 days range around the central date of each satellite time step with a 30 days/monthly running mean. The horizontal spatial representativeness error is the only remaining reference uncertainty considered in this uncertainty assessment. This error is fully described in the PVP [RD07], a summary is provided below. The spatial power spectra of SSS consistently exhibits a spectral slope of -2.4 ($S(k)=\beta k^{-2.4}$) in a range going from a few kilometres to basin scale (~10,000 km) [RD4]. The variance contained between the spatial frequency k_L and k_l (respectively, between the scales l and L , with $l < L$) is given by the double integral:



$$\sigma^2(k_L, k_l) = \iint_{k_L < k < k_l} d\mathbf{k} S(\mathbf{k}) = B \int_{k_L}^{k_l} k dk k^{-2.4}$$

Assuming three spatial scales: g for the ground truth measurements, r for the remote sensing product and L for the basin scale, $g \ll r \ll L$, $\sigma_0 = \sigma(r)$ the standard deviation of SSS contributed by all scales as measured by remote sensing, we obtain the following relationship:

$$\Delta\sigma^2(g, r) \approx \sigma_0^2 \left(\frac{r}{L}\right)^{0.4} \approx \sigma^2(r) \left(\frac{r}{L}\right)^{0.4}.$$

Assuming $L = 5000$ km, with $r = 25$ km for the SSS product, the spatial representativeness is estimated as follow:

$$\Delta\sigma_{space} = \sigma_0 * 0.35$$

With $\sigma_0 = \sigma(r)$ the CCI SSS field temporal standard deviation in time for each grid cell.

3.4 Quality metrics

Two types of quality metrics have been used throughout this document:

- Standard statistics: **mean** and **standard deviation (std)**. It assumes the central limit theorem can be assumed to produce normally distributed estimates;
- Robust statistics based on ranking which are robust against deviation from a normal distribution assumption: **median** and a robust standard deviation (**std***) scaled from the InterQuartile Range (IQR) by a factor 27/20 assuming a normal distribution.

PVP [RD1] recommends to discard points with less than 30 samples. In the following, two approaches have been followed. If one can estimate significance of an hypothesis (e.g. bias), values which are significant at 95% are indicated with dots. For the standard deviation, where there is no related hypothesis, points calculated with less than 30 samples are shown with hatching. The mean and median are considered significant for values higher than 1.96 (at 95%) of the standard errors of mean and median respectively. The confidence interval estimates for the mean and median follow the same approach. The confidence interval estimates for the standard deviation and the robust standard deviation based on IQR use a random resampling of the data (python astropy.stats.bootstrap method). For readability, the number of figures has been restricted and limited, when necessary, to the robust statistics (median and robust standard deviation based on IQR) which are more representative of the majority of the distribution.

Standard Error of the Mean is estimated following:

$$sem = \frac{\sigma}{\sqrt{N}}$$

Standard Error of the Median is estimated following:

$$sem_{median} = \frac{\sigma}{\sqrt{\frac{2(N+2)}{\pi}}}$$

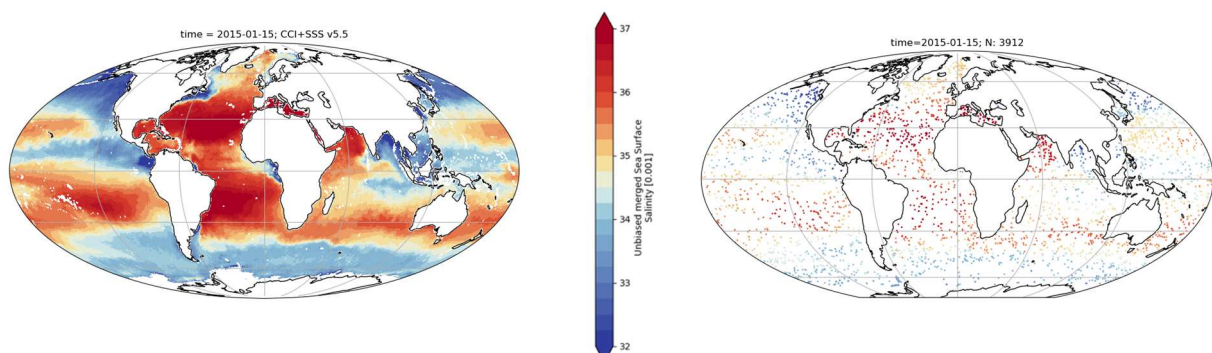
4 Validation of Products, Stability, Resolution and Product Uncertainty Estimates

In this section, we present a systematic validation with a focus on the CCI L4 version 5 product. It is compared to the CCI L4 v4 products. Section 4.1 describes the accuracy and precision of the products, including case studies at high latitude in North Atlantic and in the Arctic; section 4.2 analyses their stability and section 4.3 analyses the in situ vertical representativeness error. The effective temporal and spatial resolution are assessed in section 4.4. The quality of uncertainty estimation is assessed in section 4.5.

4.1 Accuracy & Precision

4.1.1 Global products validation for L4

SSS are presented in the top panels of Figure 4-1 centred on 15th of January 2015 for the CCI+SSS monthly product and all Argo profiles top measurements. Although the two subplots of the top panel are difficult to compare as Argo profiles are point wise measurements and CCI provides an SSS field, there is a good agreement between the two sets of observations. The satellite derived product enables mapping the gradient which is difficult with Argo point measurements. The subplots in middle panel represent the temporal median of CCI and of the gridded MDB over the full time period [2010-01 to 2023-12]. There is very good agreement in the resolved patterns between the two fields. In the gridded MDB field, some areas are insufficiently sampled (less than 30 grid points) particularly in some coastal areas affected by river plumes (e.g. Amazon) or enclosed seas (e.g. Caribbean Sea, maritime continent, Mozambique channel), and in the open ocean in the middle of the subtropical gyres or at high-latitude (Arctic and Southern Oceans). The temporal variability observed by CCI and Argo is represented on the lower subplots of Figure 4-1 using the robust standard deviation. The high variability regions (e.g. in the vicinity of the Amazon and Congo plumes, Northern Indian Ocean, the ITCZ, or the Gulf Stream) are distinct in both the CCI and gridded MDB. However, the high variability observed at high latitudes (e.g. Brazil-Falkland/Malvinas Convergence Zone, Agulhas return current, Gulf Stream) with Argo floats is not totally reproduced by the CCI products. Part of this SSS variability might occur at finer spatial resolution than sampled by the satellites (<50 km) and this effect is expected to be more pronounced at high latitude where the mesoscale is at finer scale than at low latitudes.



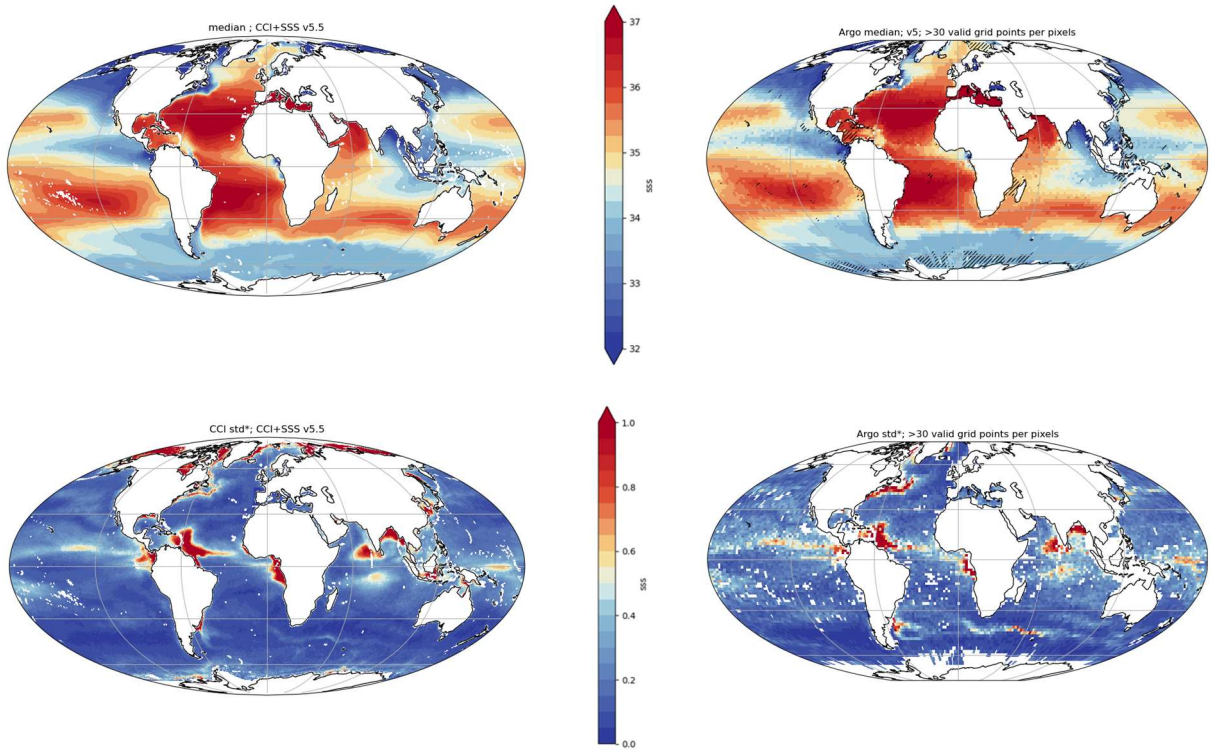
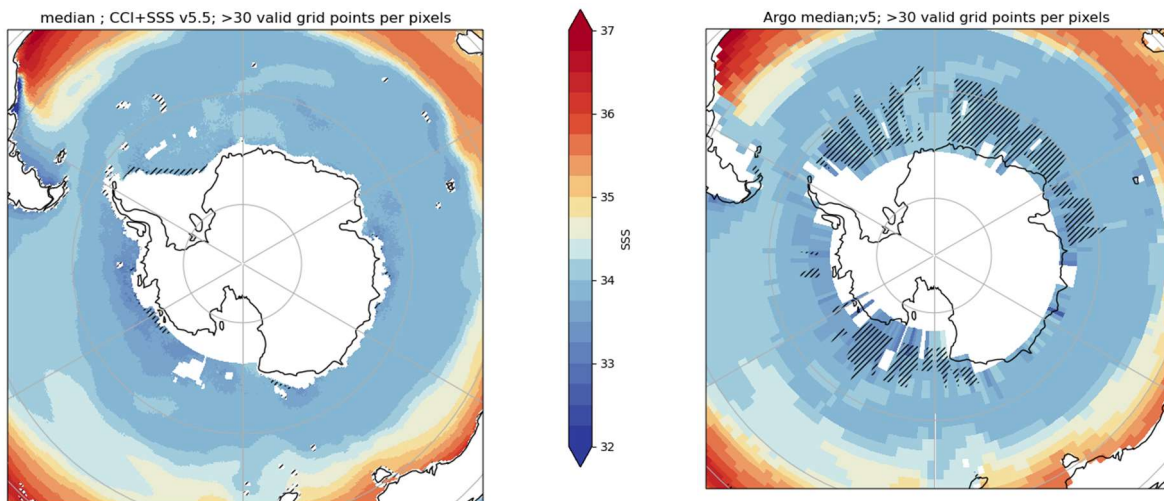


Figure 4-1: (top-left) L4 CCIv5 monthly SSS for the 15th of January 2015, (top-right) Argo salinity measurements from the Pi-MEP MDB for the same month. (middle/bottom-left) temporal median/robust standard deviation of L4 CCIv5 SSS and (middle/bottom-right) temporal median/robust standard deviation of the gridded MDB SSS. Diagonal hatching indicates regions with less than 30 points over the full time-series.



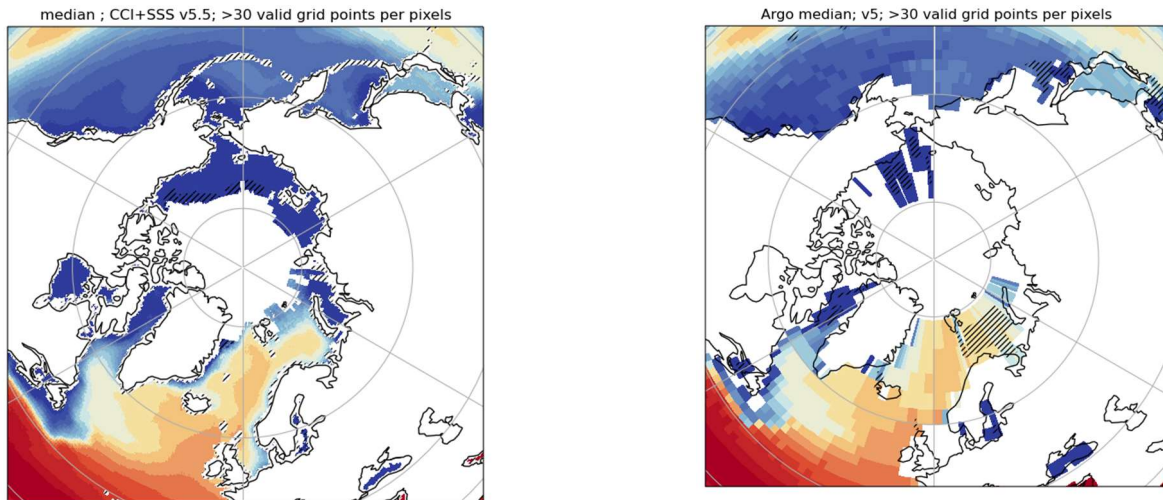


Figure 4-2: temporal median for Antarctic (top) and Arctic (bottom), of (right) Argo gridded MDB SSS and (left) L4 CCIv5 SSS. Diagonal hatching indicates regions with less than 30 points over the full time-series.

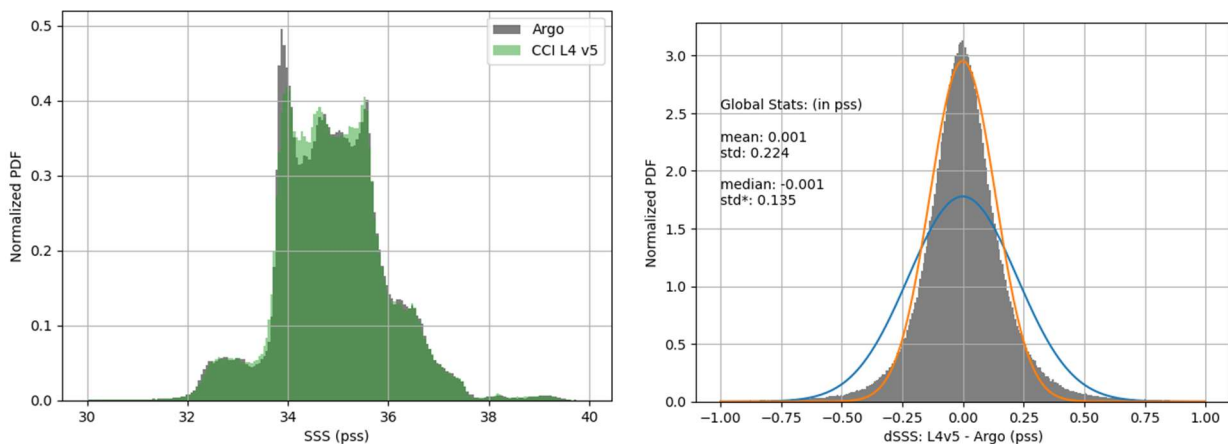


Figure 4-3: Histogram of all pairwise gridded MDB (left) Argo SSS in grey and CCI L4 v5 SSS in green; (right) Gridded MDB of the CCI L4 v5 minus Argo difference, (blue line) normalized probability function (PDF) using computed mean and standard deviation, (orange curve) normalized PDF using computed median and robust standard deviation.

The distributions of the gridded MDB of pairwise CCI L4 and Argo SSS are very similar (Figure 4-3-left) over the full range of SSS from 30 pss to 40 pss. The peak in the distribution ~ 34 pss is well resolved for CCI L4 v5 and compares well with the distribution peaks of Argo. The distribution of the gridded MDB of pairwise CCI difference against Argo (Figure 4-3-right) highlights the absence of bias ($< |0.01|$ pss), and a robust standard deviation of 0.14 pss (0.22 pss for the classic standard deviation). The difference between the robust and classic standard deviations is due to the non-normal distribution of the data difference (longer tails). The gridded pairwise measurements of Argo and CCI present a square of the Pearson correlation coefficient (R^2) of 0.97.

A comparison of Pi-MEP using the exact same Argo float colocations for v5 and v4 Monthly products are summarised in Table 3. V5 is very similar to v4 when compared to Argo. Statistics are reported in Table 3. There are particular improvements for two specific conditions:

- [C7a: distance to coast < 150 km] with particular reduction in the bias;



- [C9c: SSS > 37 pss] with particular reduction in the bias and square correlation coefficient (explained variance).

There is slight degradation for one specific condition:

- [C8a: SST < 5°C] with increase in the standard deviation and square correlation (explained variance);

Table 3: Statistics for Pi-MEP MDB comparison dataset for v4 and v5 using exactly the same Argo floats collocation. Cf Pi-MEP reports for the details about the conditions criteria.

Condition	Nobs	Median		Mean		Std*		std		R2	
		V4.4	V5.5	V4.4	V5.5	V4.4	V5.5	V4.4	V5.5	V4.4	V5.5
all	1,146,592	0.00	0.00	0.00	0.00	0.15	0.15	0.24	0.24	0.974	0.975
C1	382,616	0.00	0.00	0.00	0.00	0.13	0.12	0.16	0.16	0.970	0.971
C2	802,216	-0.01	0.00	0.00	0.00	0.15	0.15	0.23	0.23	0.975	0.976
C3	5,664	0.03	0.03	0.03	0.03	0.20	0.20	0.27	0.27	0.952	0.954
C4	211,729	0.03	0.03	0.04	0.05	0.20	0.19	0.35	0.34	0.975	0.976
C5	876,318	0.00	0.00	0.00	0.00	0.14	0.14	0.20	0.20	0.978	0.978
C6	217,763	0.00	0.00	0.00	0.01	0.23	0.22	0.34	0.34	0.968	0.969
C7a	77,070	-0.03	-0.01	-0.03	-0.01	0.24	0.23	0.37	0.37	0.991	0.991
C7b	494,235	0.00	0.00	0.00	0.00	0.17	0.17	0.27	0.27	0.956	0.957
C7c	574,350	0.00	0.00	0.00	0.00	0.13	0.13	0.17	0.17	0.967	0.968
C8a	119,525	0.01	0.01	0.01	0.01	0.18	0.19	0.31	0.33	0.924	0.917
C8b	274,999	0.01	0.01	0.01	0.01	0.15	0.15	0.22	0.22	0.978	0.978
C8c	750,643	-0.01	-0.01	-0.01	0.00	0.15	0.15	0.23	0.22	0.972	0.973
C9a	64,022	0.05	0.06	0.08	0.09	0.21	0.20	0.53	0.52	0.976	0.977
C9b	1,036,197	0.00	0.00	0.00	0.00	0.15	0.15	0.21	0.21	0.942	0.943
C9c	46,373	-0.05	-0.04	-0.06	-0.04	0.16	0.15	0.21	0.20	0.930	0.935

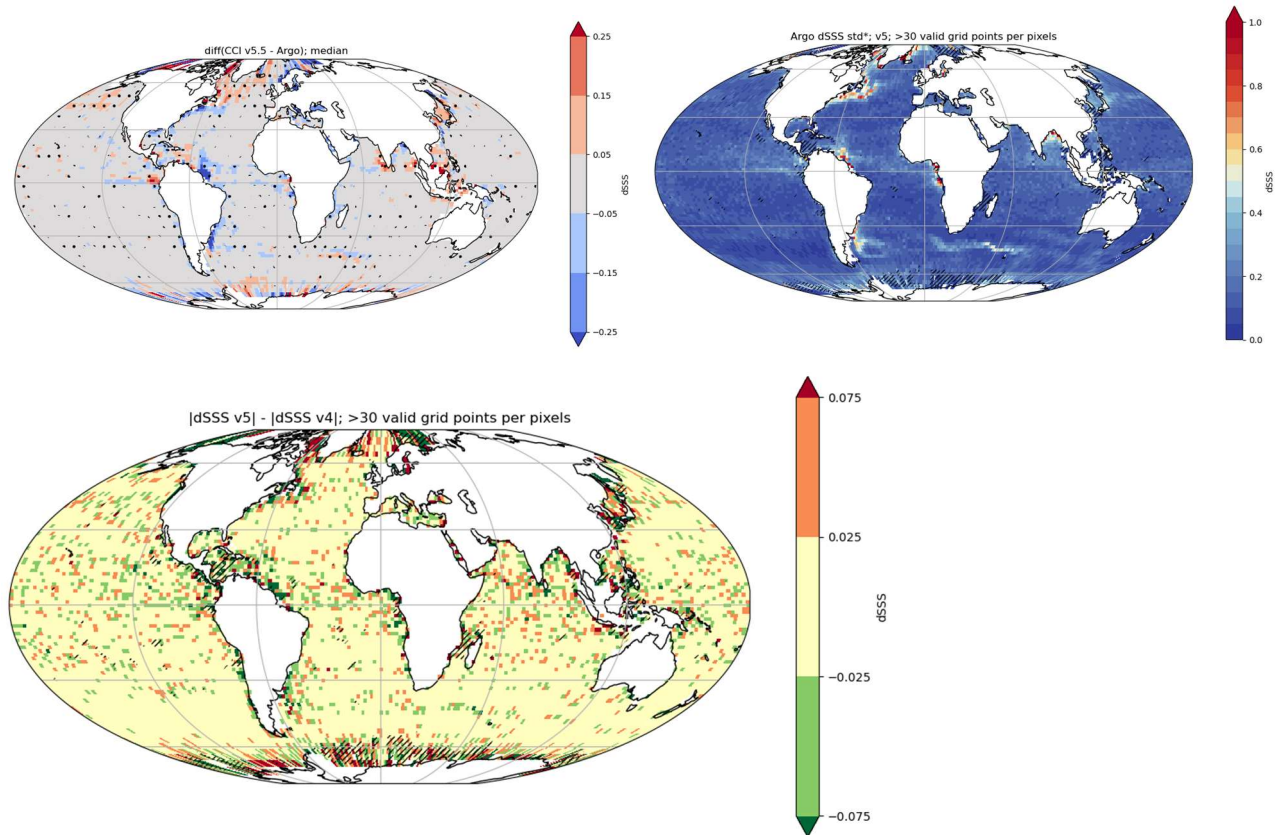


Figure 4-4 (top-left) Temporal median and (top-right) temporal robust standard deviation of gridded pairwise SSS differences between CCI and Argo. (on the left) A moving window of 2 pixels in longitude and latitude is applied to the median in order to highlight statistical significance (at 95%) which are indicated with dots. (on the right) Robust standard deviation calculated with less than 30 valid grid points in time are hatched. (bottom) differences of the temporal median differences between CCI and Argo between version 5 and version 4 using the comparison dataset.

To further assess the agreement between datasets, Figure 4-4 presents the temporal average (median) and the robust standard deviation of the gridded MDB v5 for the differences between CCI and Argo. At large scale (open ocean), the median difference is within ± 0.05 pss and the robust standard deviation difference is below 0.2 pss. There is no large scale systematic spatial difference versus Argo. Small portions of the North Pacific present significant salty bias higher than 0.05 pss. The other significant differences are in the vicinity of strong SSS gradients or strong current. Close to the coast, major river plumes appear fresher (blue) in CCI. Close positive/negative differences are observed in the Gulf stream and Agulhas return current where meanders are common, suggesting differences between Argo and satellite sampling and spatial representativeness (pointwise measurement versus 50 km pixel). These higher discrepancies between CCI and in situ are also visible in the spread, with a temporal robust standard deviation of the differences higher than 0.4 pss at these fronts, in coastal areas and river plumes (Amazon plume, Bay of Bengal, ...). Figure 4-4-bottom represents the improvements in green and degradation in orange of the median difference against Argo between version 5 and version 4, using the gridded MDB comparison dataset (*compv5* and *compv4*). This figure highlights there is no systematic and large-scale difference and most of the ocean appears yellow, i.e. no difference higher than ± 0.025 pss.



Pi-MEP statistics of CCI L4 v5 against TSG, drifters and mammal's data with the C1 criterion are reproduced in Table 4. As highlighted in section 3.1.1, the time series of CCI SSS in each pixel is calibrated by comparing a quantile of the statistical distribution of CCI SSS with the one from ISAS SSS (ISAS 2017 up to 2017 and ISAS NRT afterwards). Whereas TSG and drifters data are included in ISAS NRT, they are fully independent from ISAS 2017. Statistics of CCI data against TSG and drifters are in the same range as for Argo. Whereas some datasets present biases in absolute term higher than 0.05 pss (in order: saildrone, tsg-ncei), tsg-legos-dm, tsg-gosud, tsg-polarstern, and drifters are within ± 0.01 pss. The robust standard deviation of the difference between CCI and in situ measurements is the same between Argo and Drifters (0.12 pss) but stay close to the Argo performance (< 0.15 pss) for tsg-legos-dm, tsg-gosud, tsg-legos-survostral and tsg-polarstern. The explained variance (R2) is higher than Argo for, in order, drifters, tsg-gosud-sailing-ship, tsg-gosud-research-vessel confirming the good performance of CCI L4v5 against independent measurements.

Table 4: Statistics of CCI L4 v5.5 30dr against in situ data for the global ocean applying criteria C1 (only pairs where $RR=0$ mm/h, $3 < U < 12$ m/s, $SST > 5^\circ\text{C}$, distance to coast > 800 km). From Pi-MEP

	Nobs	Median	Mean	STD	RMS	R2	STD*
argo	407674	0	0	0.16	0.16	0.969	0.12
tsg-legos-dm	641587	-0.01	-0.01	0.18	0.18	0.968	0.14
tsg-gosud-research-vessel	309844	0	0	0.17	0.17	0.973	0.13
tsg-gosud-sailing-ship	193510	0	0	0.15	0.15	0.978	0.13
tsg-samos	138540	0.03	0.05	0.24	0.25	0.944	0.16
mammal	17512	0.04	0.06	0.35	0.35	0.731	0.17
drifter	793027	-0.01	0.02	0.21	0.21	0.986	0.12
tsg-legos-survostral	48873	0.03	0.02	0.14	0.14	0.563	0.13
tsg-ncei-0170743	76139	0.11	0.1	0.16	0.19	0.92	0.16
tsg-polarstern	63545	0	-0.01	0.2	0.2	0.958	0.14
saildrone	112787	0.17	0.22	0.38	0.44	0.74	0.29
tsg-csic-utm	163003	0.02	0.02	0.21	0.21	0.949	0.16
ices	109	-0.03	-0.02	0.19	0.19	0.687	0.13

4.1.2 Arctic Case Study

The following section provides one independent case study focussing on the Barents Sea within the Arctic using ICES database. Polar regions are especially difficult for satellite measurement due to both sea ice contamination (signal to noise ratio) and the lower sensitivity of L-band in cold waters.



4.1.2.1 Arctic Case Study: Comparison with ICES (Nordic Seas and Barents Sea) data base - Nicolas Kolodziejczyk

The Barents Sea is a test bed for CCI+SSS Arctic products as in this region, the thermohaline Polar Front (around 76°N) marks the transition between the fresh and cold Arctic Water found in the northern part, and the warm and salty Atlantic Water recirculating in the Barents Sea. The ability of CCI+SSS Arctic v5.5 product to retrieve SSS across the Polar Front, especially in northern cold water, provides a good indicator of the robustness of the dataset.

We compute 77705 colocations to the positions of the ICES (www.ices.dk) profiles between 0 and 10 meters depth in the Barents Sea and between 2010-2022 (Figure 4-5-top). In situ SSS lower than 15 on the Practical Salinity Scale PSS-78 (pss, hereafter) are considered as outliers and are discarded because they may be associated with small-scale localized and intense freshening smaller than the satellite footprint that may bias the validation. The products are validated for the Summer and Fall periods, i.e. from June to December. The ICES in situ data are mainly located west of 40°E (Figure 4-5-top). For the CCI+SSS dataset, the differences to the in situ SSS range mainly from -0.5 to +0.5 pss. Scattering the CCI against the ICES SSS (Figure 4-5-middle) reveals a significant agreement ($R^2=0.51$) with no significant bias, especially during summer (August-September, in yellow-orange in (Figure 4-5), when the SSS in Barents Sea ranges from 32 pss to more than 35 pss.

Overall, at low temperature (less than 4°C), both SSS difference shows a larger dispersion (Figure 4-5-bottom). It remains to understand whether this larger dispersion in may stem from a remaining issue in the dielectric constant parameterization, or from some other artifacts, such as a remaining sea ice contamination in L-Band radiometric data.

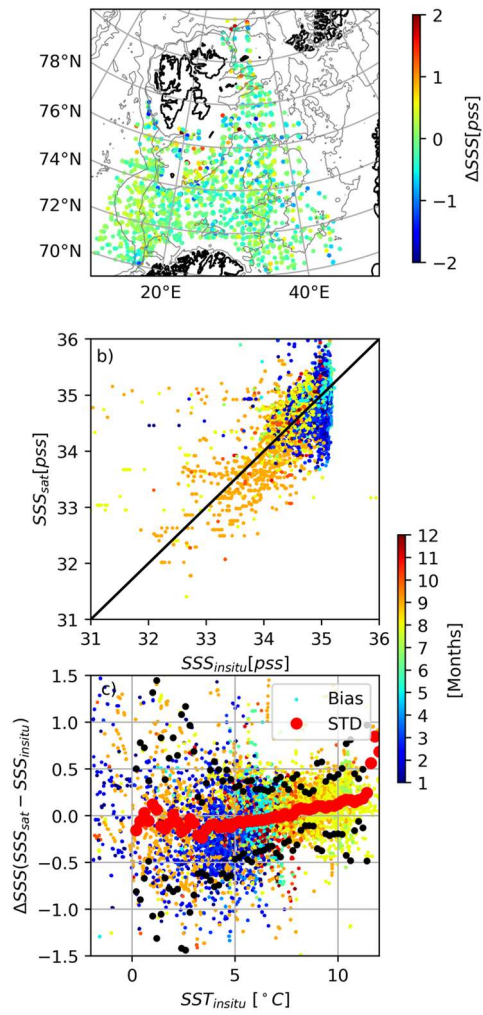


Figure 4-5 (top) SSS difference between CCI+SSSv5.5 Arctic product and ICES in situ measurements between 2010-2022 in the Barents Sea; (middle) Scatter plot between CCI+SSSv5.5 and in situ measurements; (bottom) SSS difference as a function of the in situ SST (in $^{\circ}C$).

4.2 Time series stability: intra-annual & long-term stability

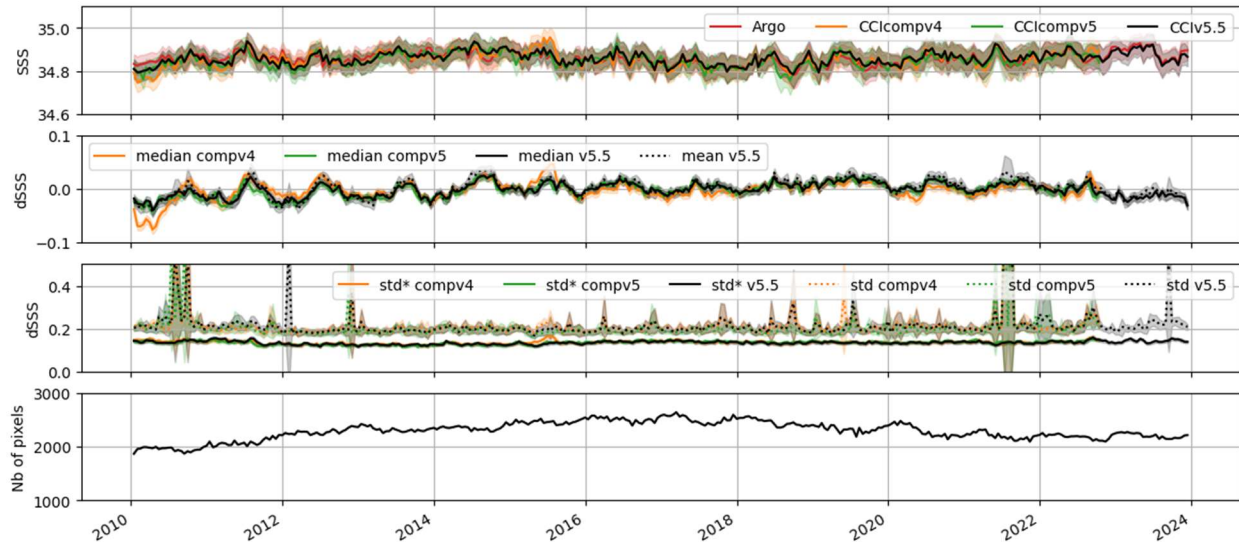


Figure 4-6: (1st panel): mean SSS of gridded MDB of pairwise Argo in red and L4 CCI in black for v5 and in orange and green for comparison v4 and v5; (2nd panel) Average of; (3rd panel) standard deviation of; the gridded MDB of the pairwise SSS difference between CCI and Argo. Solid lines represent (2nd panel) the median (3rd panel) the robust standard deviation. Dashed lines represent (2nd panel) the mean (3rd panel) the standard deviation. The shading indicates the 95% confidence interval. (4th panel) number of valid gridded MDB values.

The time series in Figure 4-6 represents the temporal evolution of gridded MDB of the pairwise measurements of CCI L4 (v5, compv4 and compv5) and Argo and their differences. The mean SSS temporal variability represented on the top panel shows good agreement between CCIv5 (CCIv5.5 in the label) and Argo (collocated against v5) with a mean around 34.9 pss. The beginning of the period in 2010 highlights a lower value for CCI than Argo, but with an improvement for v5 compared to v4. In April to August 2015 there is an increase of SSS for v4 against Argo, which is linked to known issue in SMAP v5.0 in North Atlantic. In v5, this issue has been solved. Except the two elements mentioned above, there are no other significant differences between *compv4* and *compv5*.

The two middle panels represent the gridded MDB of the pairwise differences of CCI with Argo for average difference (mean and median); and dispersion (classic standard deviation and robust standard deviation). The global, temporal difference remains within ± 0.05 pss. There is a small but appreciable global seasonal cycle with a minimum at the beginning of each year. The amplitude decreases with time, in particularly since 2016. Similarly, to the previous panel, strong differences are observed at the beginning of the period in 2010 and in April to August 2015. There are significant differences between *compv4* and *compv5* from the beginning to mid-2010, between end of 2011 and beginning of 2012, between April to August 2015 and at the beginning of 2020.

The dispersion, as estimated by the robust standard deviation of the difference, stays relatively constant over the full time series between 0.13 pss and 0.16 pss. There is a diminution of the robust standard deviation in mid-2011 with Aquarius and a local peak for *compv4* in mid-2015 corresponding to the known issue with SMAP v5.0 in North-Atlantic. The classic standard deviation presents some peaks suggesting more extreme values in the tail of the distribution.

Globally, the three CCI L4 versions are very similar. The number of valid pixels in the gridded MDB for each time step (bi-weekly) is indicated in the bottom panel. It slightly increases in time from 2010 to 2016 directly link to the increase of the number of Argo profiles.

The temporal variability of the gridded MDB of the pairwise CCI/Argo differences is further assessed using latitude-time (Hovmöller) plots over the global ocean (Figure 4-7) for the L4v5 products. About half of the pixels are not significantly different from zero (at 95%). There are significant oscillating signals with stronger amplitudes at higher latitude. There is a strong difference in mid-2015 between 40°-80°N linked to the known issue with SMAP v5.0 between April and August 2015. The first 6 months in 2010, indicates CCI are fresher than Argo particularly in the Northern hemisphere and at high latitudes. There is a small trend from fresher (blue) to saltier for latitudes between 0°N and 30°N. A symmetric trend exists in the southern hemisphere.

Figure 4-8 is similar to Figure 4-7, but using the gridded MDB comparison dataset for v4 and v5, and showing at the bottom the improvements (in green) and degradation (in orange) between v4 and v5. This latter figure highlights the strong improvement in the correction of the difference between CCI and Argo in the first 6 months in 2010 and during April to August 2015 linked to the known issue with SMAP v5.0 which was used in CCI v4. Some degradations appear sporadically at latitude higher than 40°N.

The spatial representation of seasonal climatology of the gridded MDB v4 difference (Figure 4-9), does not highlight strong, significant and large-scale differences. It is calculated using the median for each season over the full time series. Around Japan and in the northern North-Atlantic, CCI L4v4 is fresher in Winter (DJF) and saltier in Summer (JJA). A seasonal spatial signature is less pronounced and significant in the Southern hemisphere. Some local seasonal differences are visible close to the coast, generally related to river plumes, potentially associated with vertical stratification (see details in section 4.3).

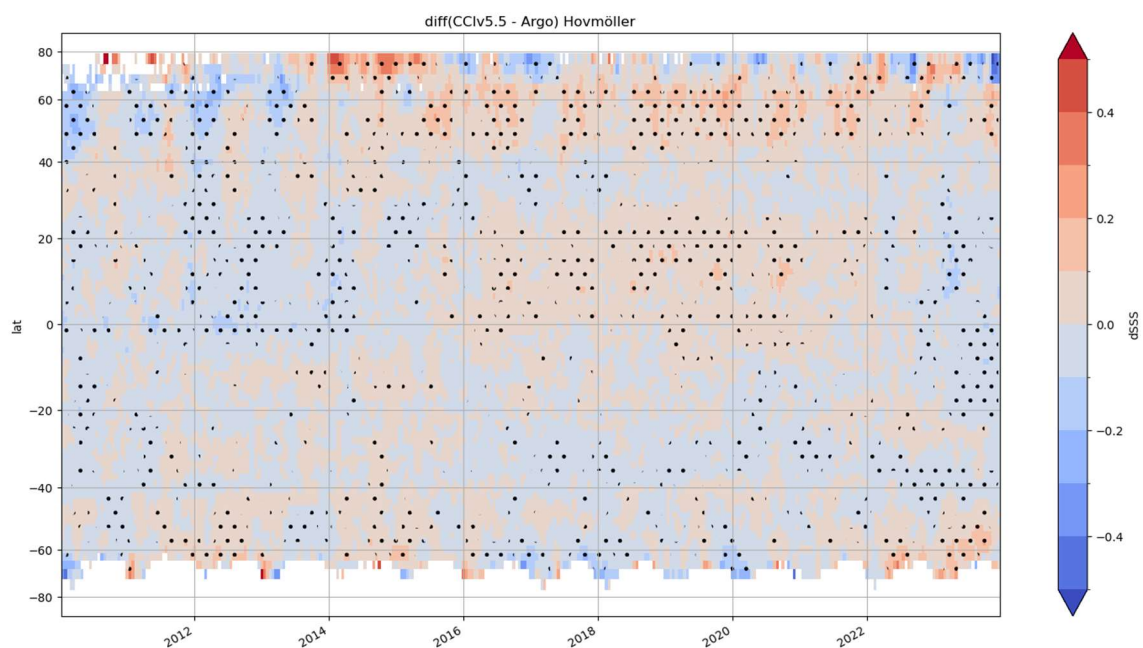


Figure 4-7: Global latitude-time Hovmöller of the gridded MDB of the pairwise CCI difference with Argo for L4 v5. Each pixel represents the median value after a moving window over 2 pixels in latitude and time. Data which are significantly different from 0 (at 95%) are indicated with dots. All sub-figures share the same colour bar.

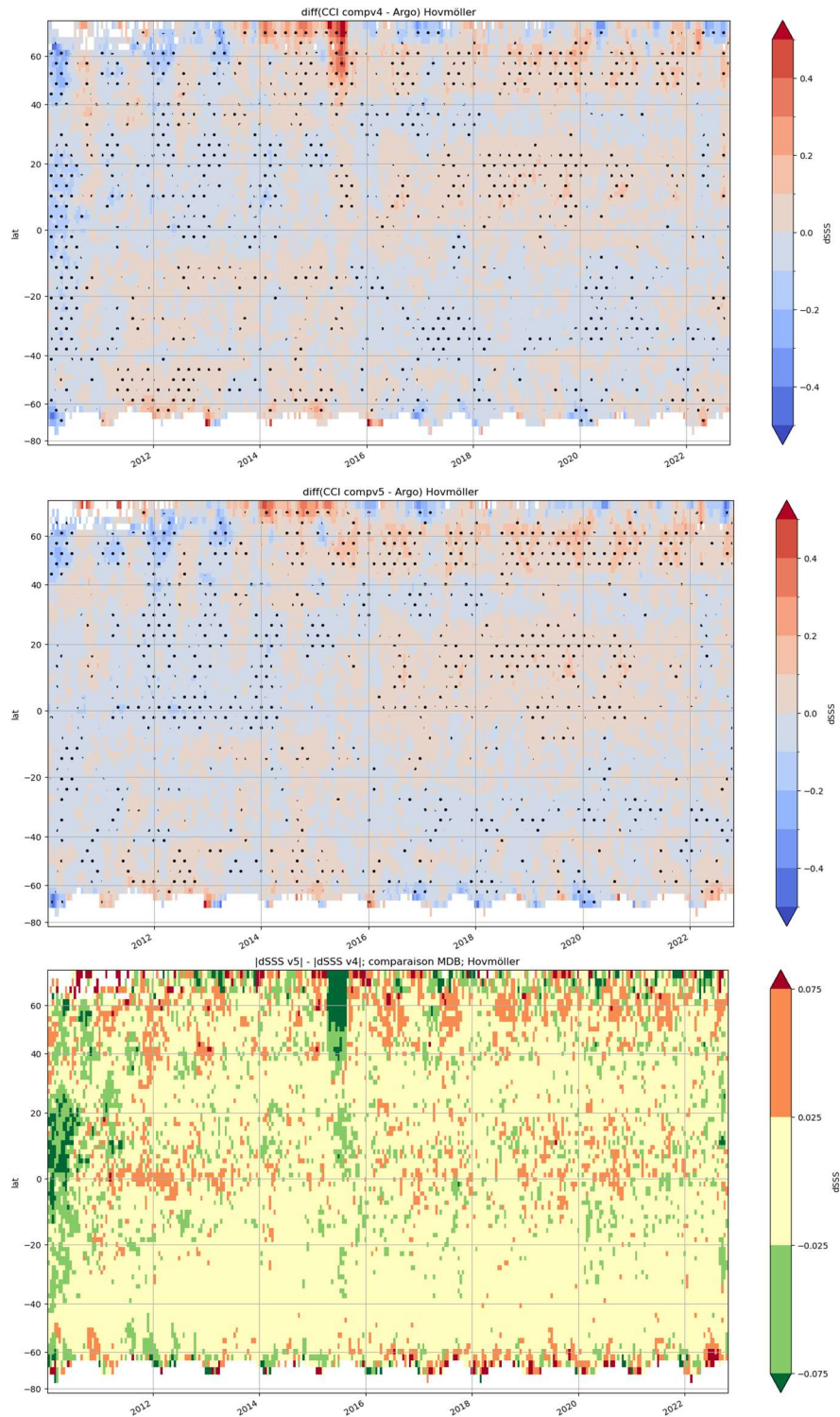


Figure 4-8: Global latitude-time Hovmöller of the gridded MDB of the pairwise CCI difference with Argo for (top) L4 v4 comparison dataset; (middle) L4 v5 comparison dataset; (bottom) Absolute difference between the two subplots above. Green indicates improvement towards zero; Red indicates degradation away from zero. Each pixel represents the median value after a moving window over 2 pixels in latitude and time. Data which are significantly different from 0 (at 95%) are indicated with dots. All sub-figures share the same colour bar.

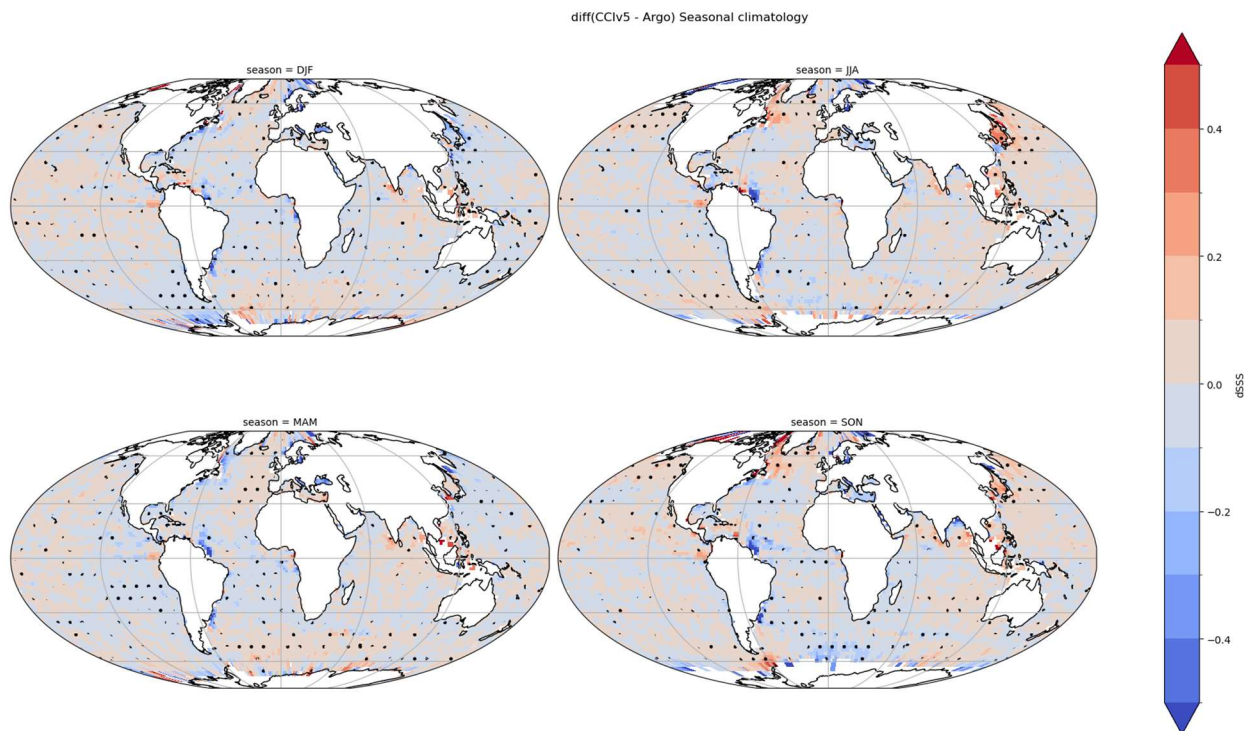


Figure 4-9: Seasonal climatology of the gridded pairwise CCI L4 difference with Argo calculated using the median. A moving window average of 2 x 2 pixels in longitude and latitude have been applied to increase the number of sampled, hence the significance. Pixels, which are statistically significant (at 95%) are indicated with dots.

4.3 In Situ Vertical Representiveness Error

The skin depth of satellite measurements depends on the wavelength; at a frequency of 1.4 GHz, the skin depth is about 1 cm. In most situations, this depth is expected to represent the top few meters of the ocean. However, significant differences between the surface ocean and a few meters depth have been observed in some regions either for a few hours (typically 1 to 5 hours, depending on wind conditions) after heavy rainfall (Boutin et al., 2016; Supply et al., 2020), or in river plumes where large differences can be found between the top meter and a few meters depth (e.g. Supply et al., 2020).

In order to get a global distribution of the vertical representiveness error, we calculate the gradient for each Argo profile between an acquisition depth of 5 m and 10 m. We use the same grid as for the pairwise comparison and take the median value of this gradient for each cell (in time and space). The seasonal climatology of this gradient in salinity is represented in Figure 4-10 highlighting that most of the ocean does not show a noticeable gradient between 5m and 10m, except in areas with strong freshwater fluxes (e.g. river plumes, ITCZ, Labrador current, ...). As expected, the value at 5 m is usually fresher than the salinity at 10 m. The surface is saltier only for very specific areas and periods such as the Mediterranean Sea in Summer. The strongest gradients in salinity relate to the tropics in all seasons with typical values higher than 0.02 pss/m. If we linearly extrapolate these high gradients from 5 m to the surface, we might suspect differences due to the vertical sampling exceeding 0.1 pss. In Summer, vertical gradients appear in the Northern Hemisphere in the vicinity of western boundary currents (Gulf Stream and Kuroshio).

These results suggest the SSS measured by satellite would tend to be fresher than the one measured *in situ* by Argo. However, this effect is an order of magnitude less than the seasonal one observed on Figure 4-9 so that the mean difference of CCI minus Argo in Figure 4-9 does not reflect the patterns below.

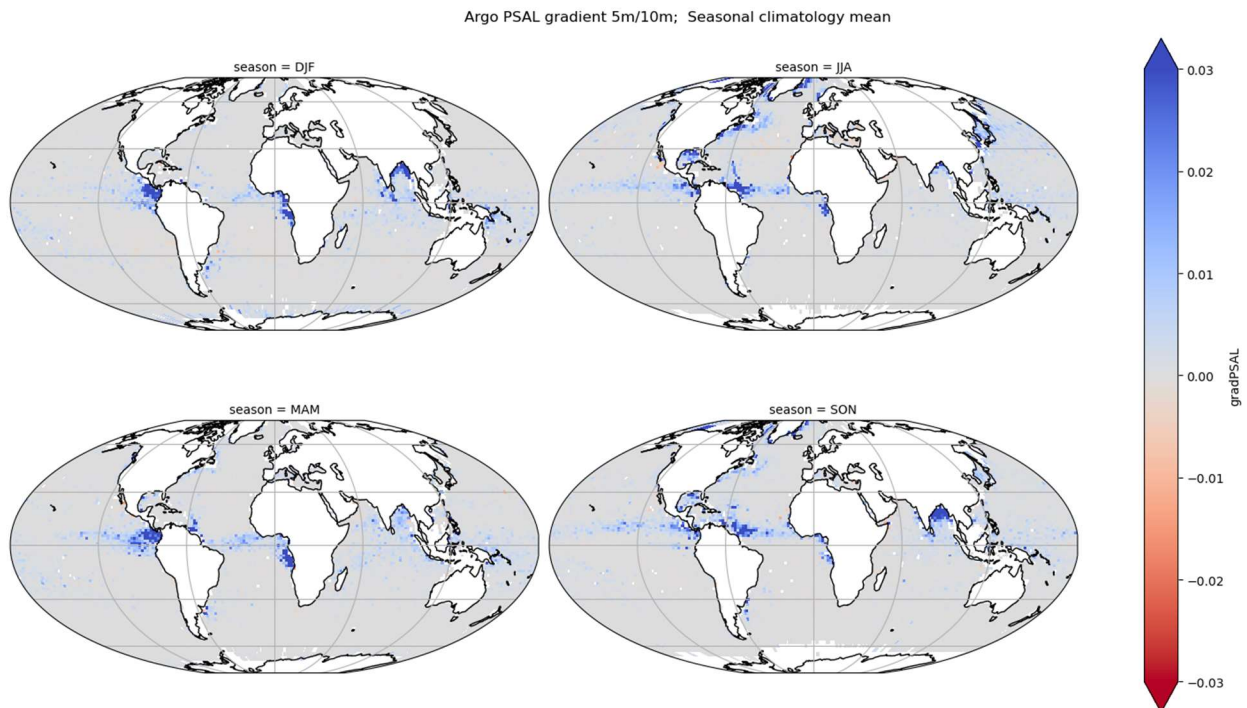


Figure 4-10: Seasonal Salinity gradient (in pss/m) derived from Argo at 5 m and 10 m. Gradient are gridded on the same grid as used for the pairwise difference (bi-weekly; 175 km).

4.4 Temporal & spatial effective resolution

4.4.1 Temporal effective resolution

The average temporal power spectra of SSS from all moorings and CCI collocations from the Pi-MEP MDB are represented in Figure 4-11 for the weekly products and in Figure 4-12 for the monthly products. ISAS optimal interpolation SSS and the SSS from the Mercator numerical circulation model are also shown. CCI L4 Weekly and Monthly products shows as expected a decrease at the Nyquist frequency (respectively 14 days and 60 days).

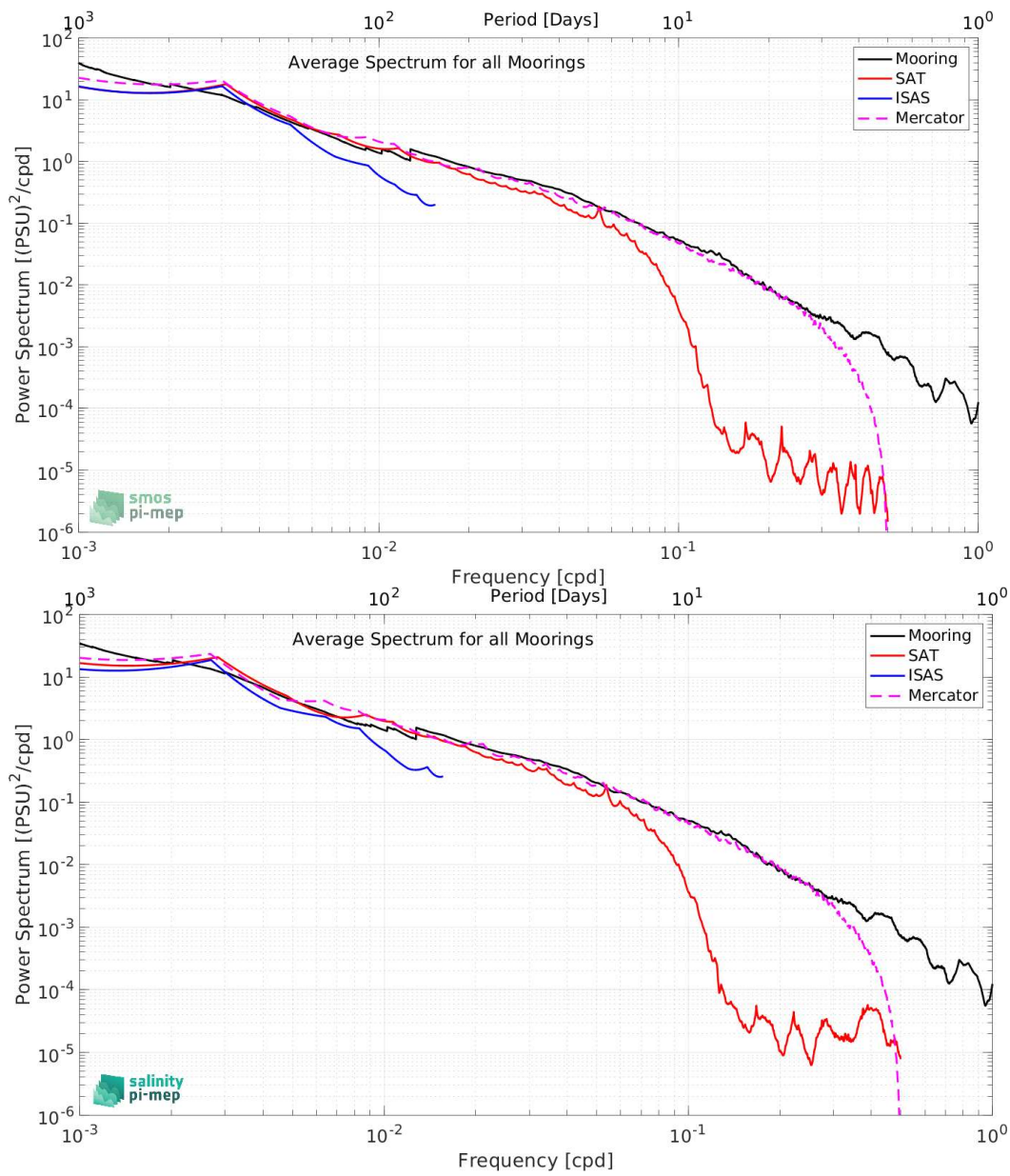


Figure 4-11 : Average power spectrum of SSS from (black) moorings, (red) CCI Weekly products, (blue) ISAS, (pink) Mercator; (top) for CCI L4 Weekly v4.4; (bottom) for CCI L4 Weekly v5.5. from Pi-MEP.

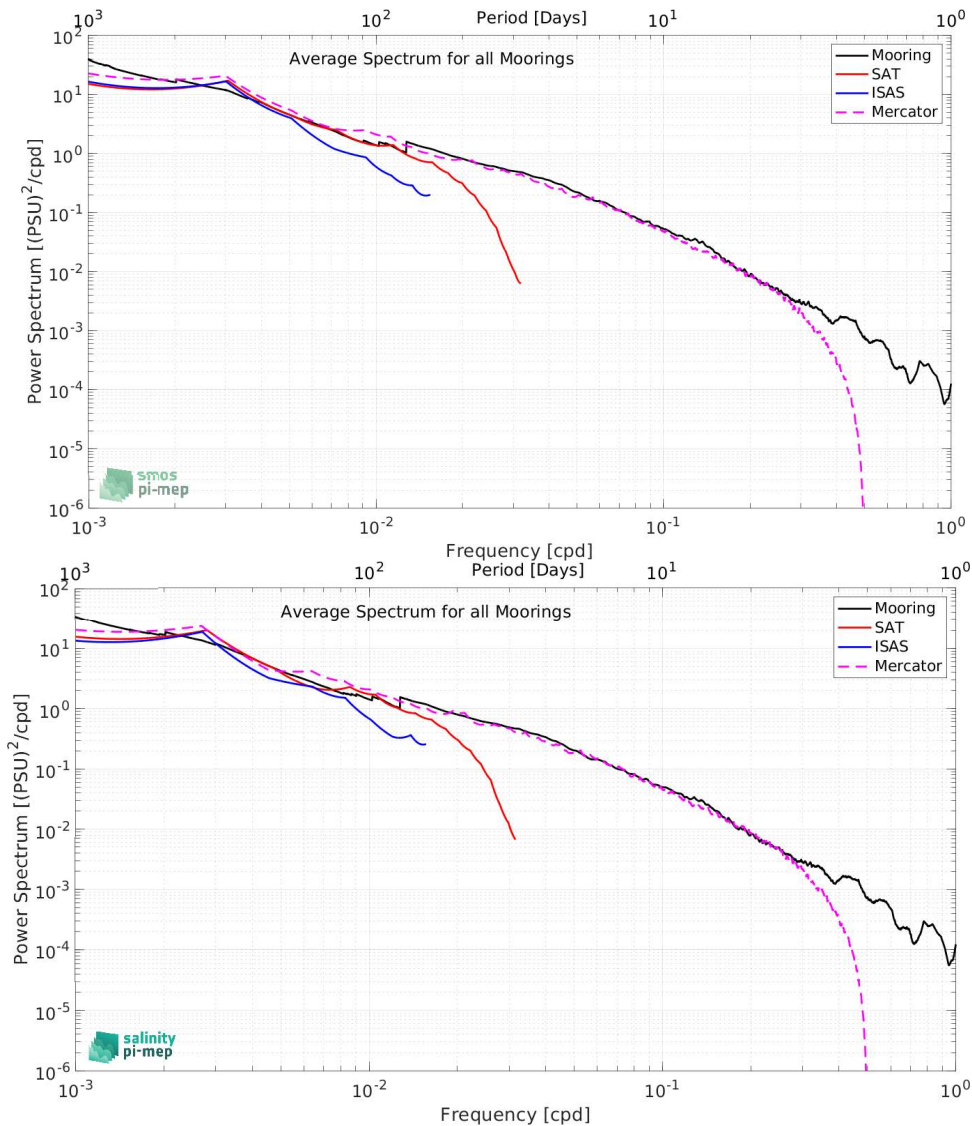


Figure 4-12: Average power spectrum of SSS from (black) moorings, (red) CCI Monthly products, (blue) ISAS, (pink) Mercator; (top) for CCI L4 Weekly v4.4; (bottom) for CCI L4 Weekly v5.5. from Pi-MEP.

4.4.2 Spatial effective resolution: Assessment of mesoscale features in Tropical Atlantic

The surface mixed layer thermohaline structures at meso-scale to submesoscale (smaller than the local radius of deformation, *Chelton et al.*, 1998) are ubiquitous features in the global ocean. They contribute to horizontal and vertical heat and salt exchange, and vertical re-stratification (*Fox-Kemper et al.*, 2008). They have a global impact on ocean circulation and climate since they contribute to the cascade of energy from large scale toward the smallest scales of diffusive mixing (*Callies and Ferrari*, 2013). Eventually, they have a major impact on biogeochemistry and ecosystems. The submesoscale processes are characterized by very intense vertical velocities that allow strong exchanges of carbon, oxygen and nutrient between surface and subsurface ocean (*Lévy and Martin*, 2013).

Until early 2010, satellite capabilities for observing surface thermohaline variability have mainly relied on the observation of Sea Surface Temperature (SST) only, resolving horizontal small scale features such as 10 km (Kilpatrick *et al.*, 2015). In contrast, synoptic images of Sea Surface Salinity (SSS) were not available and in situ SSS at high resolution were only available from a few high resolutions transects from Thermosalinograph (TSG) survey from ship of opportunity or cruise campaign (Kolodziejczyk *et al.*, 2015b). Since 2010, thanks to ESA SMOS mission, then NASA Aquarius and SMAP missions, 4-7 days global maps of SSS at resolution between 40-100 km are now available, permitting the observation of larger mesoscale features in subtropical and tropical region (Reul *et al.*, 2014; Kolodziejczyk *et al.*, 2015a).

In order to check the effective capability of the new CCI-SSS product (7 day) to monitor the mesoscale features of SSS in the subtropical and tropical regions, the CCI product's SSS were systematically co-localised and compared with TSG SSS along existing repeated transects in the Subtropical North Atlantic and Tropical Atlantic. An effective metric to assess the SSS horizontal variance and scale content of both products is to compute the spectra and coherency spectra between co-located TSG SSS and CCI+SSS transects (Boutin *et al.*, 2018).

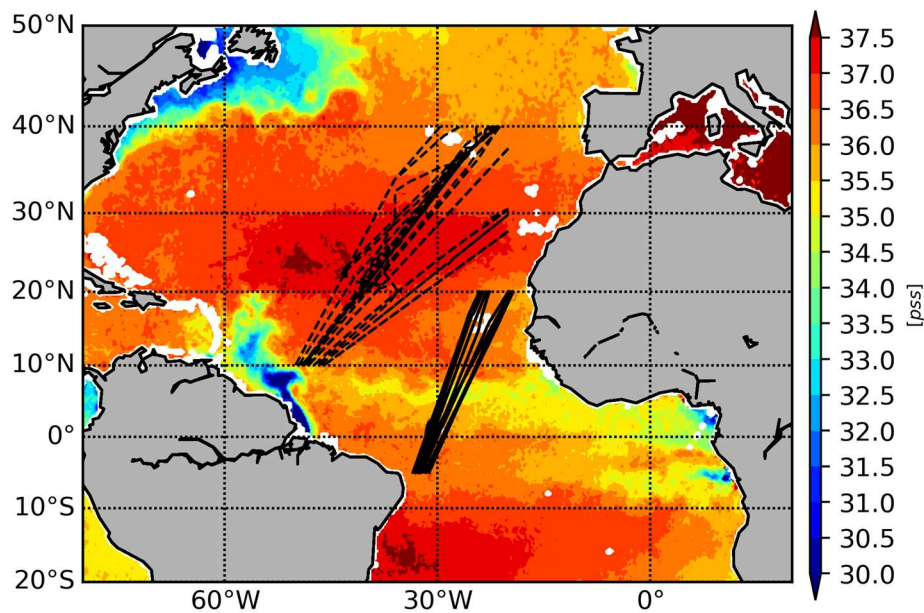


Figure 4-13: CCI+SSS on 30 June 2011 with (dashed line) 92 TSG transects in the Subtropical North Atlantic) and (solid line) 27 TSG transect in the Tropical Atlantic. All SSS transects have been carried out between 2011-2016.

SSS TSG transects were collected from ships of opportunity (representative of salinity at 10 m depth), resolving horizontal SSS features at around 2-3 km (Alory *et al.*, 2015). Two regions were chosen for the present study (Figure 4-13): i) the North Atlantic subtropical SSS maximum (50-20°W/10-40°N), where 92 transects between 2011-2016 are available; and ii) the Tropical Atlantic (40-10°W/5°S-20°N) where 27 transects between 2014-2016 are available. Individual transects were visually inspected and suspicious transects were discarded. To reduce uncertainty due to noisy individual spectrum from each individual transect, spectra were averaged for both regions.



The horizontal SSS coherency spectra refer to the coherency of the SSS horizontal variability between the co-located TSG SSS and CCI+SSS products, *i.e.* the level of correlation of the SSS signal for a given wavelength range. This allows the assessment of the actual capability of CCI+SSS products to observe and resolve mesoscale features (>50 km).

In the Subtropical North Atlantic (Figure 4-14a), in spite of slightly less energy between 50-1000 km wavelength, CCI+SSS horizontal variance spectrum, both TSG and CCI+SSS spectra show good agreement, *i.e.* comparable spectral slopes between 50-1000 km are observed. This suggests that for this range of wavelengths the variance of mesoscale features are probably smoothed in CCI+SSS products. Interestingly, the coherency exhibits a quasi-linear decrease from large scale (coherency>0.75 for wavelength > 1000 km) to mesoscale (coherency~0.30 for wavelength ~ 300 km). The significance (at 95%) is lost for wavelengths below 200 km. This suggests that wavelength smaller than 300 km are poorly represented in the CCI+SSS product. This is consistent with previous study investigating the SMOS LOCEAN CEC L3 product (*Boutin et al., 2018*) in the same region, however with a slightly better coherency for CCI+SSS product. Note the CCIv5.5 slightly performs slightly better than previous CCI+SSS version at small scale coherency between 300-200 km scale [RD09], TSG and CCI+SSS spectra show very comparable behaviours, the level of variance and slope have comparable values. Furthermore, both spectra also show a relatively high level of coherence at wavelengths larger than 300 km (coherency>0.5). In the Tropical Atlantic region, the coherency drops at wavelengths smaller than 200 km. It suggests that the CCI+SSS product is not able to consistently resolve scale smaller than 100 km. Note that the v5.5 product coherency is slightly improved in comparison of previous CCI+SSS version, resolving smaller scale beyond 200 km [RD09]. This suggests a slight improvement in the Tropical Atlantic with the v5.5 version.

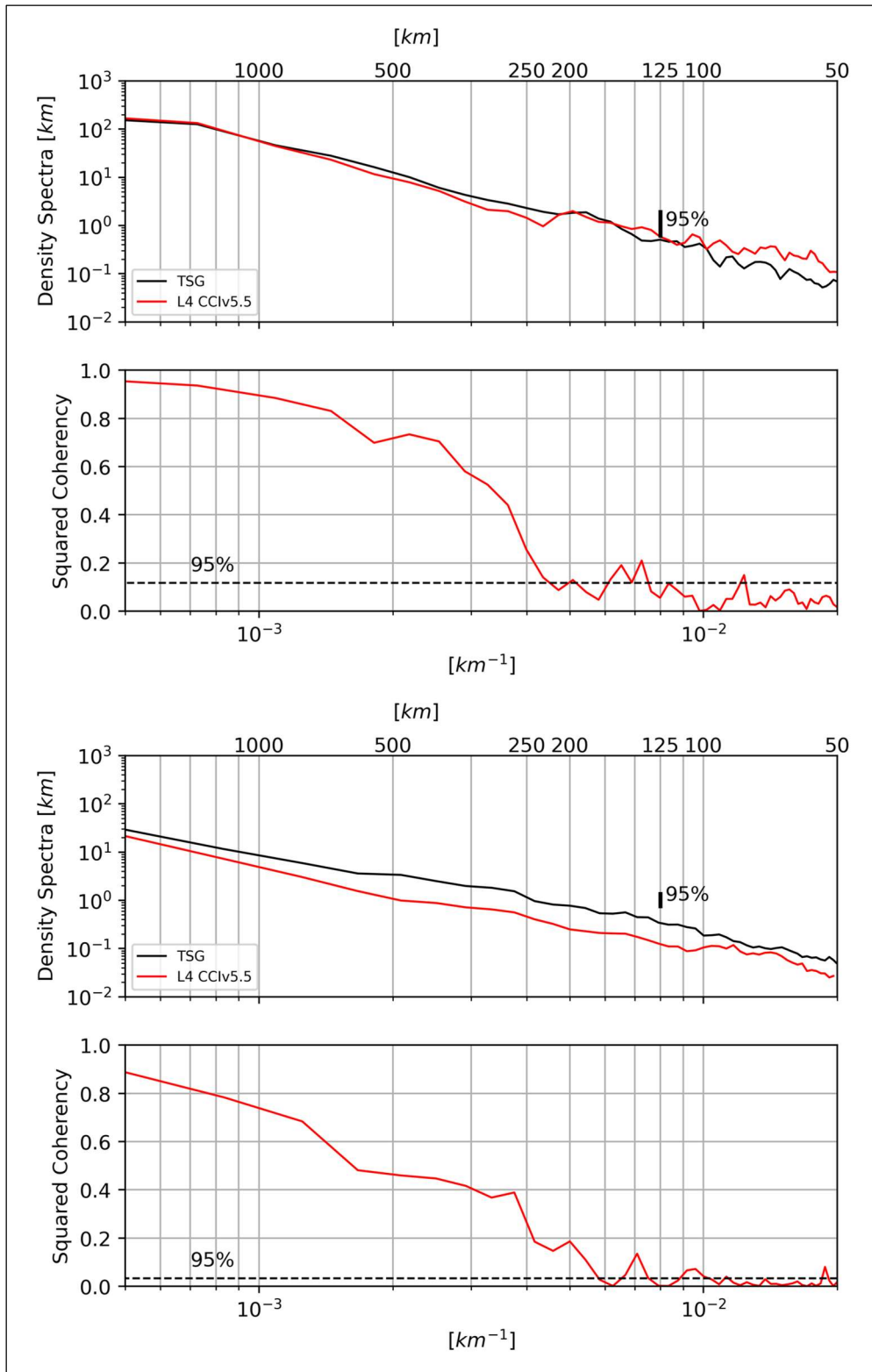


Figure 4-14: a) Density spectra from from 92 collocated TSG (black); CCI+SSS v5 (solid red) SSS transects in Subtropical North Atlantic. Vertical thick black bar is the level of confidence at 95%. b) Coherency between the TSG and CCI+SSS SSS transects. Dashed line is the level of significance at 95%. c) Density spectra from from 27 collocated TSG (black)/CCI+SSS (red) SSS transects in Tropical Atlantic. Vertical thick black bar is the level of confidence at 95%. d) Coherency between the TSG and CCI +SSS SSS transects. Dashed line is the level of significance at 95%.

In conclusion, in the subtropical Atlantic, the CCI+SSS product is able to resolve wavelengths of the order of 300 km. This wavelength corresponds to horizontal mesoscale features of the order of about 150 km (such as a large gradient or eddy). However, the level of coherency between TSG SSS horizontal variability and CCI+SSS drops rapidly at mesoscale. In the tropics the level of coherency remains high up to 300 km wavelength and then drops dramatically.

The loss of coherency at smaller horizontal wavelength could be explained by i) the limited resolution of SSS satellite mission (>50 km), ii) the remaining noise and artifacts in the CCI+SSS data, and iii) smoothing from objective analysis procedure of the CCI+SSS products. Nevertheless, it is worth pointing that inconsistency between instantaneous and point-wise measurements from the TSG data and co-localized CCI+SSS products (7 days, 50 km) may be responsible for shifts and lags between TSG SSS measurements and CCI+SSS products SSS along transects, resulting in loss of coherency for the smaller and faster SSS mesoscale structures.

4.5 Uncertainty

As explained in section 3.3 above, we will follow two approaches to validate satellite uncertainty estimates:

- Normalise the dSSS by the uncertainty with a centred reduced variable and analyse the variation compared to a theoretical behavior of a random normalised variable with mean of zero and standard deviation of one.
- Compare the dSSS distribution with the uncertainty estimates.

For both cases, we will consider the satellite uncertainty $\Delta\sigma_{sat}$ alone or the total uncertainty which combines the satellite uncertainty with the reference uncertainty itself which includes the

horizontal representiveness error ($\sigma_{tot} = \sqrt{\Delta\sigma_{sat}^2 + \Delta\sigma_{ref}^2}$).

4.5.1 Normalised SSS

In this section we look at normalising the SSS differences (dSSS; satellite and Pi-MEP) by the uncertainties (either just satellite or satellite with reference uncertainties). In an ideal situation, with perfect estimation of the uncertainties, the normalised standard deviation would be one.

Figure 4-15 represents a time series of the normalised dSSS using (A) the CCI provided satellite uncertainties and (B) the quadratic mean of the satellite uncertainties plus the reference uncertainties described in the methods. The normalised SSS represented in (Figure 4-15A bottom rows) shows a standard deviation between one and two when the normalisation uses just the satellite uncertainties. Inclusion of the Aquarius is clearly seen in the timeseries with a step following launch in June 2011. The end of mission for Aquarius (June 2015) is not as obvious, perhaps due to the proximity (in time) to the launch of SMAP (April 2015). In mid-2015, there is a blob in std for *compv4* which is linked to the known issues from SMAP v5.0 seen above. Over the period 2010 to 2015, *compv5* is closer to one than *compv4* with no sensible difference afterwards. The robust standard deviation always gives slightly lower estimates compared to the classic standard deviation due to longer tails in the distributions. The higher values observed here are linked to the reference uncertainties linked to differences between pointwise measurements and pixel-averaged measurements. With the total uncertainties in (Figure 4-15B bottom),

including the reference representativeness error, standard deviation are closer to one, even slightly below one for the SMOS-only period (01/2010-06/2011).

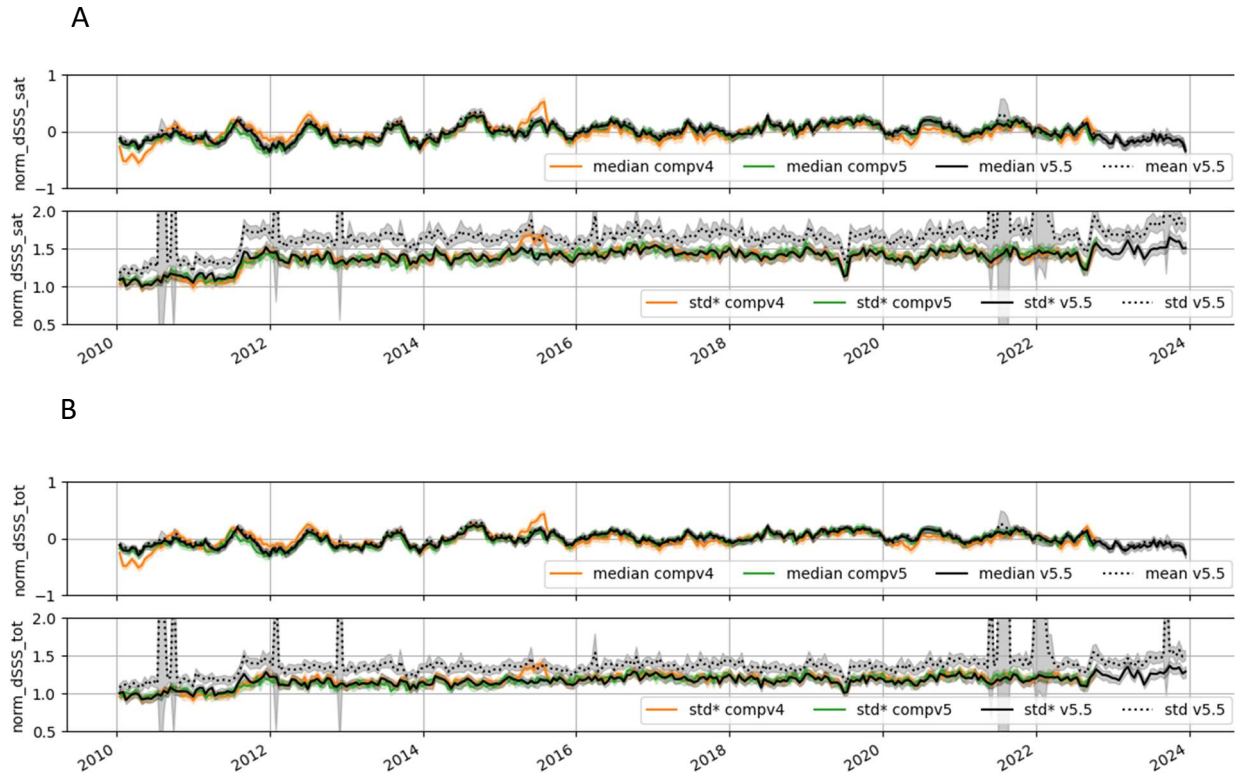


Figure 4-15 : Time series of the normalised SSS normalised using (A) the satellite uncertainty; (B) the total uncertainty combining the satellite and reference uncertainty. Top row for each panel represents (solid line) the median and (dashed line) the mean. Bottom row for each panel represents (solid line) the robust standard deviation and (dashed line) the classic standard deviation. Colours are for the L4v5 and the comparison dataset for L4v4 and L4v5.

The average (median, mean) time series of the normalised SSS (Figure 4-15 A/B 1st row) does not provide information about the uncertainty. For each point, we have more than ~2000 observations (cf Figure 4-6 last row), leading to a theoretical variability (standard deviation) of the normalised SSS of 0.02 which is much higher than what we observe.

4.5.2 Compared SSS Distribution

The gridded MDB of the pairwise differences are now binned in uncertainty 0.05 pss bins (Figure 4-16) and computed over the full time series for each product (*compv5* and *compv4*). The top row is based on satellite uncertainty whereas the bottom row reflects total uncertainty. Ideally the standard deviation (classic or robust) and the dSSS should follow a one-to-one relationship.

If one only takes into account the satellite uncertainties (Figure 4-16-top), then the observed robust standard deviation exceeds the satellite uncertainties but follows a nearly linear relation up to a satellite uncertainty of 0.4 pss for *compv4*, but tend to increase further for *compv5*. If one adds the representativeness error (Figure 4-16-bottom), all products are closer to the one-to-one relation up to a total uncertainty of about 0.4 pss. For large values of total uncertainties, *compv5* is closer than *compv4* to the one-to-one relationship.

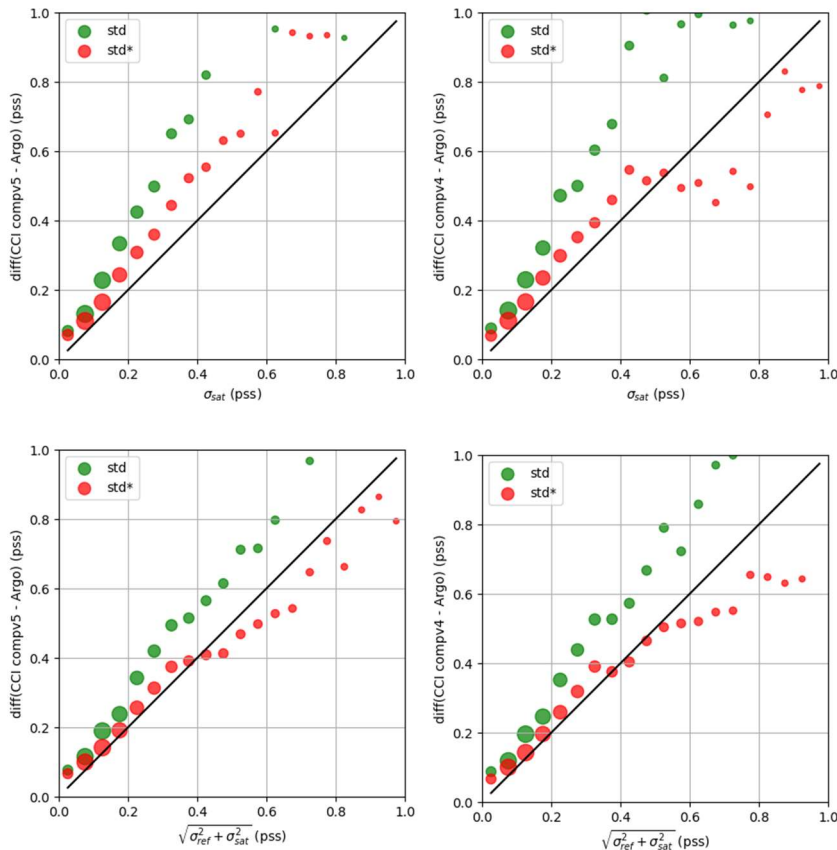


Figure 4-16: measured standard deviation (green and red dots) for classic and robust standard deviation respectively; of the gridded pairwise CCI/Argo difference (dSSS) for each uncertainty 0.05 bin. (top) using satellite uncertainty; (bottom) using total uncertainty - satellite + reference (column from left to right) for comparison dataset L4v5 and comparison dataset L4v4. The size of the circle indicates the number of data.

4.5.3 Estimation of mismatch error using GLORYS 1/12°

In this subsection, we use the Pi-MEP MDB to estimate the mismatch error using output from the GLORYS 1/12° daily model. GLORYS salinity is taken at the time, horizontal position and at two depths (0.5m depth and in situ depth) of the in-situ measurements (here Argo). To simulate coarse acquisition from satellite, average GLORYS values are taken within a radius of 12.5 km of GLORYS SSS (0.5m depth) and within 30 days around Argo float locations/time using a spatio-temporal averaging.

The difference of salinity between GLORYS resampled (12.5 km, 30 days, surface) and GLORYS at Argo depth presents some systematic differences (Figure 4-17) with negative bias, similar to the ones observed in Figure 4-4, close to large rivers plumes like Amazon, Niger, Mississippi, Bay of Bengal or for some western boundary currents like the Gulf Stream or the Brazil current. Positive bias, similar to the ones observed in Figure 4-4, are present in the Falkland/Malvinas current and in the North-western part of the Atlantic. The robust standard deviation of the mismatch difference highlights the same areas as mentioned earlier, i.e. areas characterized by strong current and/or strong SSS gradients such as river plumes, which are the same as the ones observed in Figure 4-4. For the full dataset, the mismatch bias is close to zero (-0.001 pss) with a standard deviation of 0.109 pss (robust standard deviation of 0.046 pss), which is about half to one third the difference between CCI and Argo (not shown).

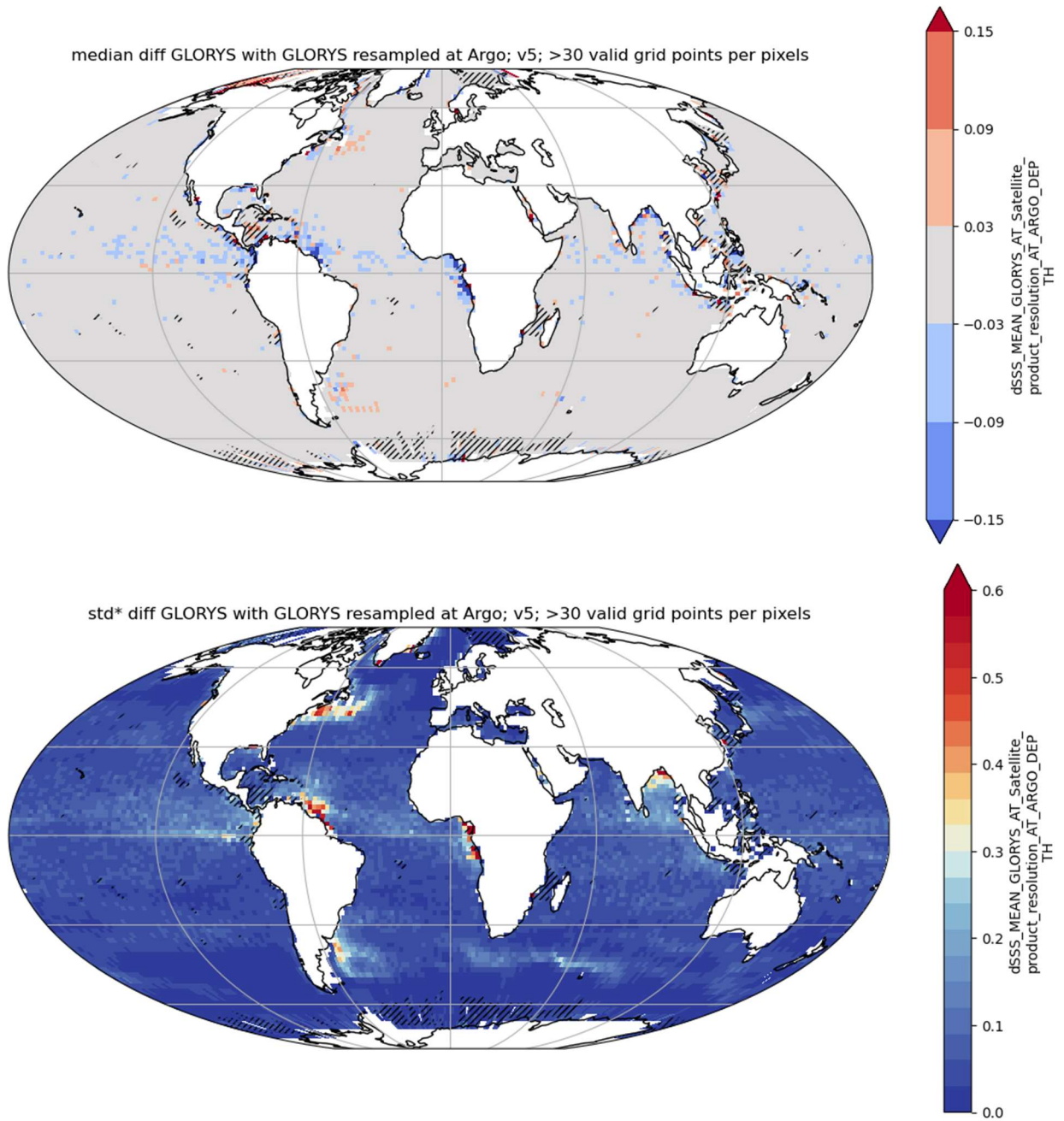


Figure 4-17: (top) Temporal median and (bottom) temporal robust standard deviation of the estimated sampling mismatch using GLORYS. This sampling mismatch estimates is obtained from the difference between GLORYS averaged over 50km, 30 days and GLORYS sampled at Argo time and position (horizontal and vertical). The colour scale is zoomed by 40% compared to the colour scale in Figure 4-4.

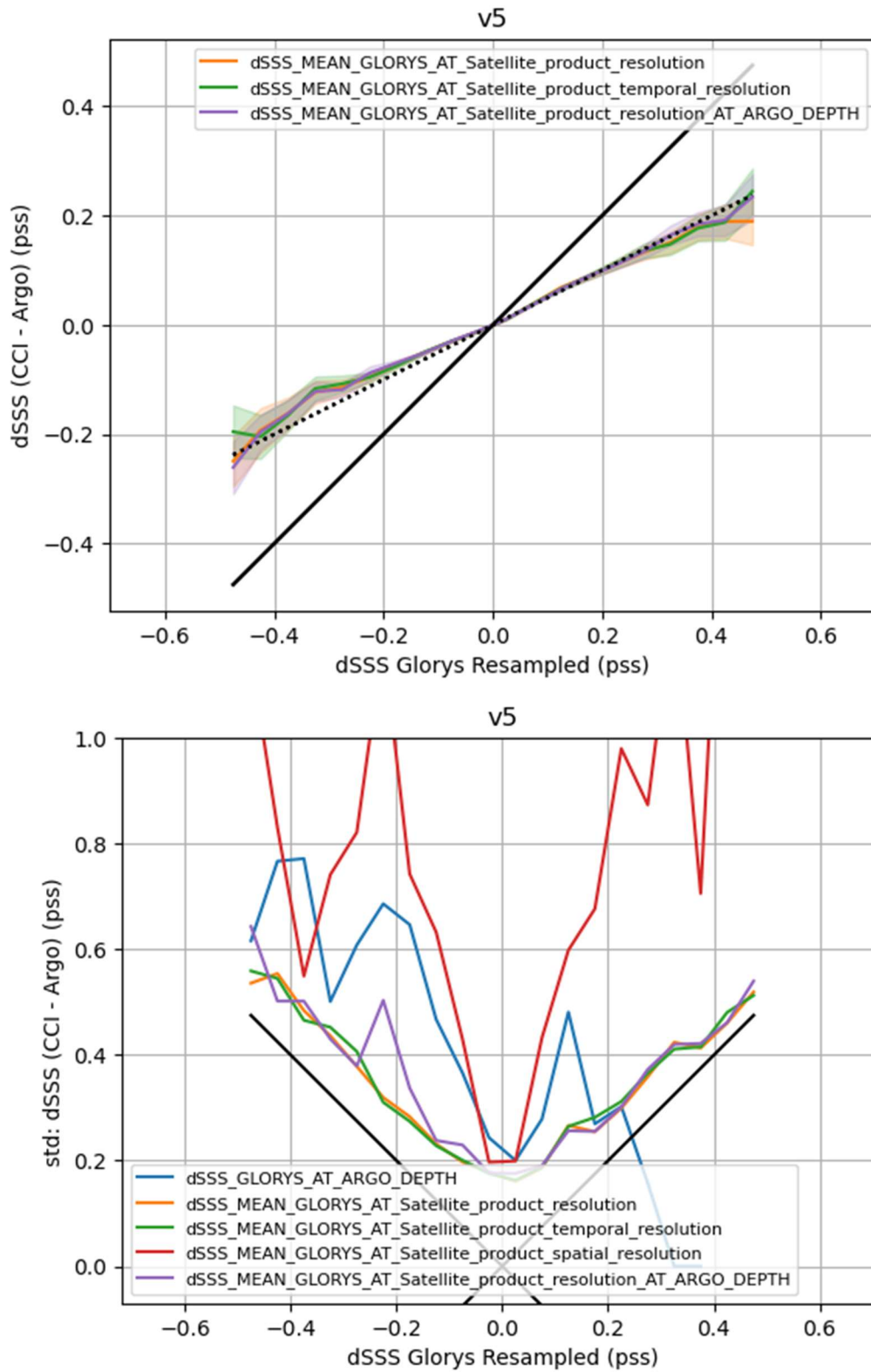


Figure 4-18: (top) mean and (bottom) standard deviation of the observed difference between CCI and Argo per bins of expected mismatch using GLORYS with the different resampling strategy represented in colour (see legend). For clarity, on the top figure, only the most significant plots are presented.



The comparison of the observed difference between CCI and Argo with the one expected by GLORYS (Figure 4-18-top panel) highlights a systematic difference which is explained by the sampling mismatch between surface and point measurements (for GLORYS resampled at 30 days – *product_temporal_resolution*, both 30 days, 12.5 km – *product_resolution*, or adding the vertical sampling at Argo depth – *product_resolution_AT_ARGO_DEPTH*). This difference explained about half the difference observed between CCI and Argo and is linear in the range ± 0.5 pss in the expected mismatch. If one resampled over 12.5 km only, or at Argo depth only (not shown), the estimate mismatch is either not significantly different from zero or does not explain the difference observed.

If one corrects for this systematic mismatch based on GLORYS and a 12.5 km, 30 days, Argo at depth sampling: i.e. $CCI - Argo - ratio * (GLORYS_{resampled} - GLORYS_{Argo})$, we obtain a standard deviation of the corrected difference between CCI and Argo of 0.219 pss (robust standard deviation of 0.132 pss), which is best for a ratio of 0.4 to 0.5.

As highlighted e.g. in [Thouvenin-Masson et al., 2022], and in Figure 4-17 the sampling mismatch between surface and point measurements play a significant role in the uncertainty. Figure 4-18-bottom represents the observed standard deviation of the difference CCI with Argo as function of the expected mismatch using GLORYS. It shows an expected vertical symmetry at zero for all resampling estimates excepted the one taking only the difference between the surface and the depth in blue. Mismatch estimates for resampling at “*product_resolution*” and “*product_temporal_resolution*” follow a one-to-one relation suggesting these spatio-temporal scale are relevant to explain the observed variability. The other curves (see legend for resampling strategy) are much steeper, suggesting they only explain one portion of the observed variability. Part of the unexplained variability could come from the remaining fine spatial resolution used here (radius of 12.5 km; 25 km diameter), which correspond to the product grid (25 km) but is about half the instrument resolution (>40 km) and about one fifth of the resolved resolution (>100 km in the (sub)Tropical North Atlantic). It could also come from the fact that the smallest scales are not well resolved GLORYS $1/12^\circ$ daily outputs. In [Thouvenin-Masson et al., 2022], in order to take the GLORYS unresolved small scales into account, the variability was increased by a factor 1.20.

To conclude this subsection, we highlight in addition to the increase uncertainty due to the sampling mismatch, there is a systematic mismatch we can correct for based on a numerical model, which improves the performance of the CCI, Argo difference by about 2%: from 0.224 pss to 0.219 pss (0.135 pss to 0.132 pss for robust standard deviation). If one limit areas where sampling mismatch estimate from GLORYS is below 0.05 pss, CCI performances against Argo is better than 0.18 pss (standard deviation), i.e. about 20% better than the global case.

Annex A Validation of C/X-band CCI Products

A1. Amazon-Orinoco river plumes

Comparison of CCI C/X-band dataset against EN4 over the Amazon-Orinoco river plumes for the 2002-2011 period (22,000 pairs) gives an overall negative mean bias of -0.1 pss (0.0 pss for the median) with a dispersion of 0.5 pss (RMSD of 0.5 pss). The CCI C/X-band dataset (black line in Figure A 1) as a lower dynamic to SSS resulting in positive biases against in situ (here EN4 and CORA) at low salinity. The spatial bias and dispersion in Figure A 2 follow the main position of the river plume. The positive bias over this fresh salinity area is consistent with results from Figure A 1. The full time series over the Amazon-Orinoco river plumes box (Figure A 3) gives a dispersion about twice as big during the C/X-band period (2002-2010) with a value of 0.5 pss than during the L-band period starting from 2010 with 0.2 pss.

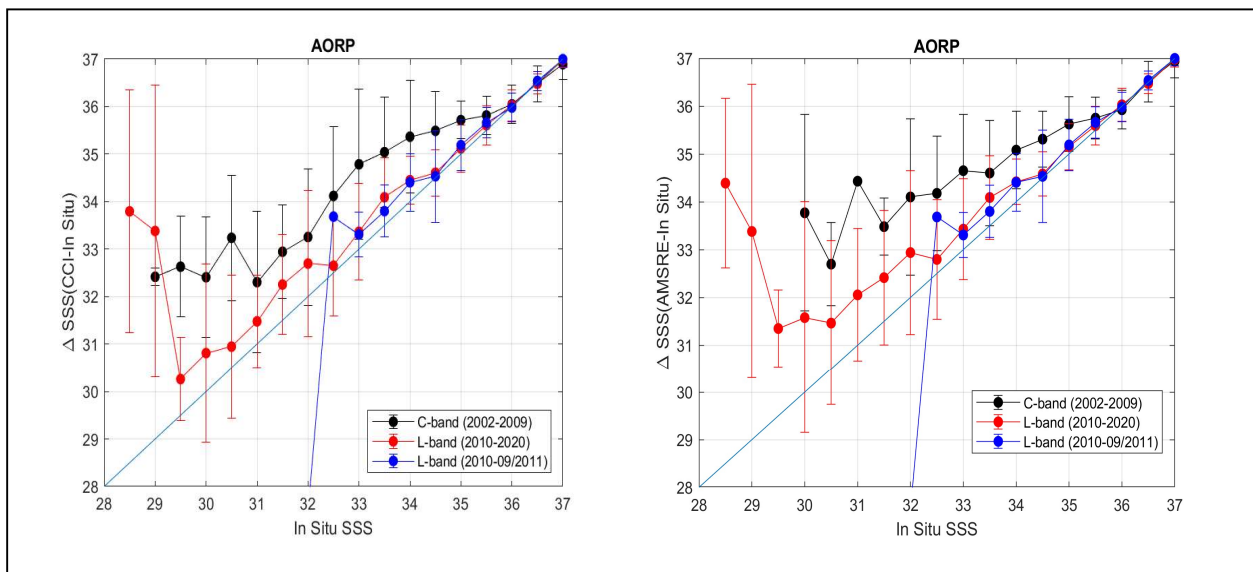


Figure A 1: Pairwise comparison between CCI C/X-band and in situ measurements from (left) EN4 and (right) CORA datasets

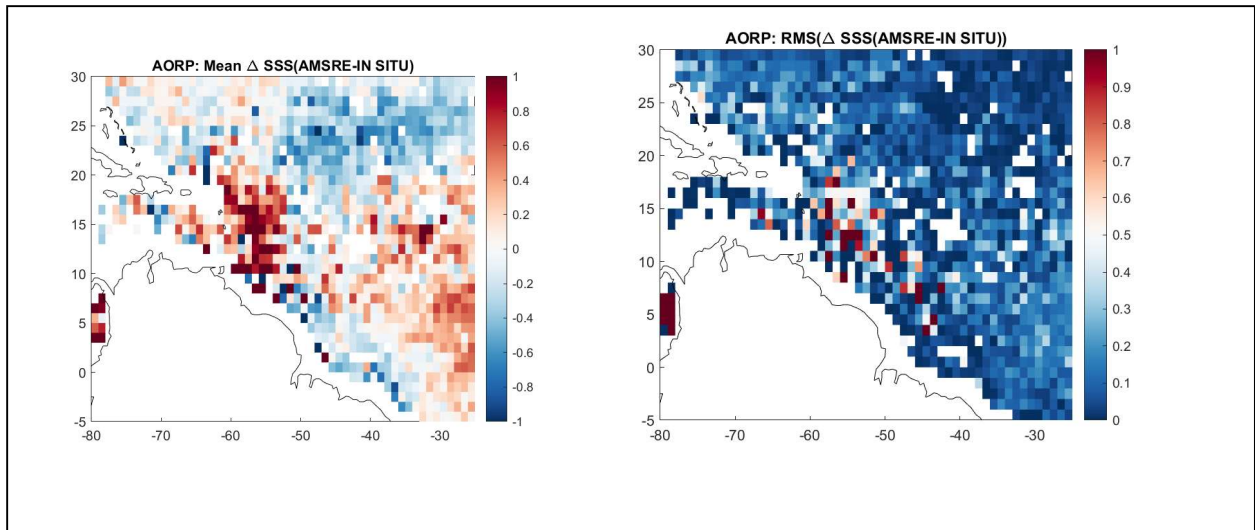


Figure A 2: Pairwise comparison between CCI C/X-band and in situ measurements on a $1^\circ \times 1^\circ$ grid and showing (left) the mean difference and (right) the RMSD.

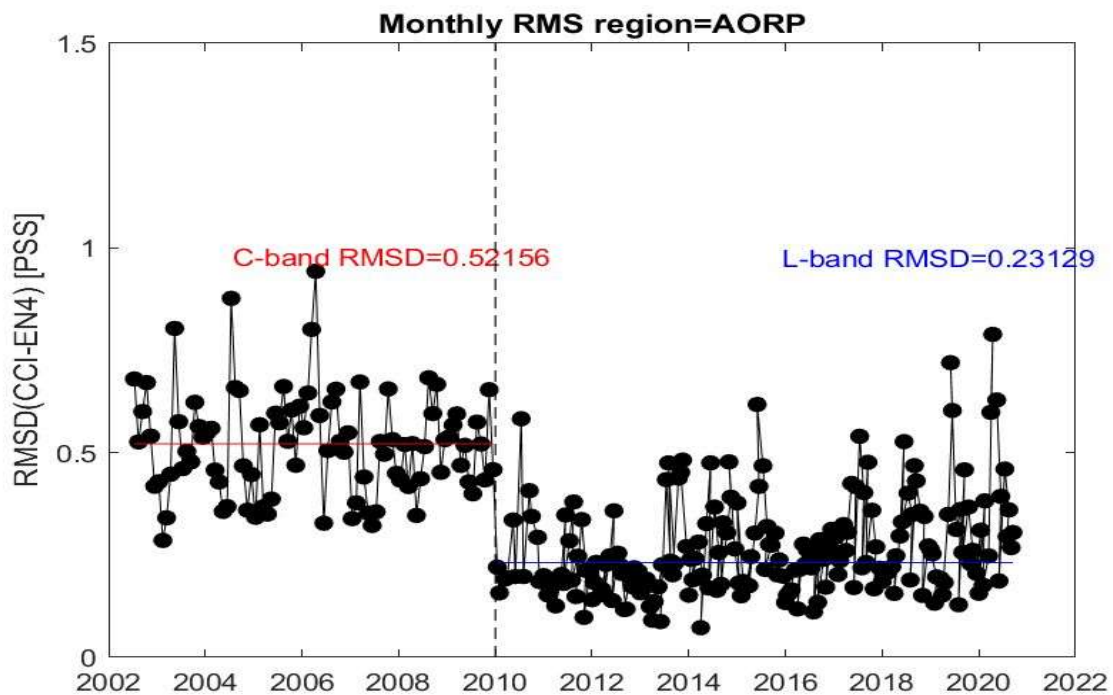


Figure A 3: Time series of the RMSD against EN4 over the Bay of Bengal for the full time series including the C/X-band and L-band period.

A2. Niger-Congo river plumes

Comparison of CCI C/X-band dataset against EN4 over the Niger-Congo river plumes for the 2002-2011 period (9,900 pairs) with no overall mean bias (0.1 pss for the median) with a dispersion of 0.5 pss (RMSD of 0.5 pss). The CCI C/X-band dataset (black line in Figure A 4) as a lower dynamic to SSS resulting in positive biases against in situ (here EN4) at low salinity. The spatial bias and dispersion in Figure A 5 follow the main position of the river plume. The positive bias over this fresh salinity area is consistent with results from Figure A 4. The full time series over the Niger-Congo river plumes box (Figure A 6) gives a dispersion larger during the C/X-band period (2002-2010) with a value of 0.4 pss than during the L-band period starting from 2010 with 0.3 pss.

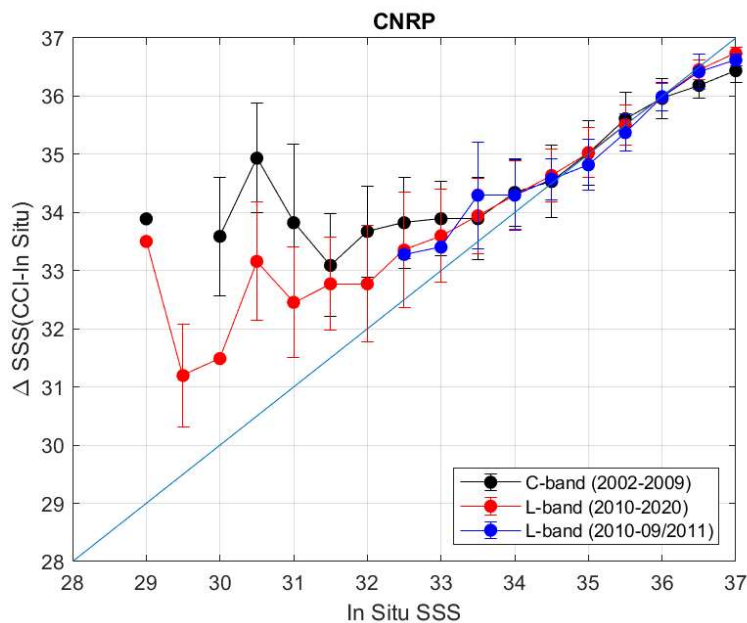


Figure A 4: Pairwise comparison between CCI C/X-band and in situ measurements from EN4 dataset.

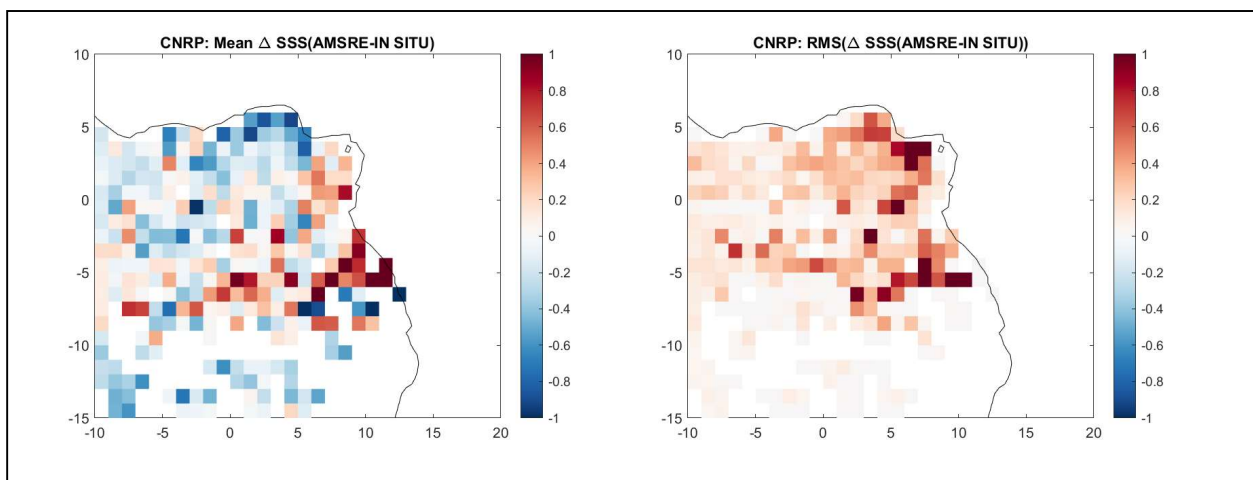


Figure A 5: Pairwise comparison between CCI C/X-band and in situ measurements on a 1°x1° grid and showing (left) the mean difference and (right) the RMSD.

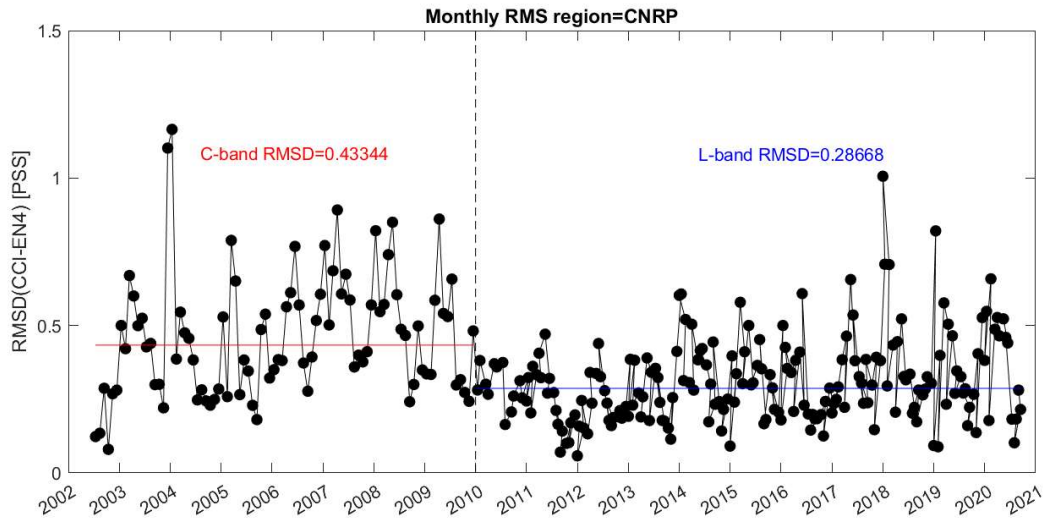


Figure A 6: Time series of the RMSD against EN4 over the Bay of Bengal for the full time series including the C/X-band and L-band period.

A3. Mississippi river plumes

Comparison of CCI C/X-band dataset against EN4 in the Mississippi river plumes for the 2002-2011 period (500 pairs) gives an overall negative mean bias of -0.3 pss (0.0 pss for the median) with a dispersion of 1.0 pss (RMSD of 1.0 pss). The dataset is very limited and makes difficult to give solid conclusion. CCI C/X-band dataset (Figure A 7) show little correlation with in situ SSS (here EN4). The spatial bias and dispersion in Figure A 8 follow the main position of the river plume. The positive bias over this fresh salinity area is consistent with results from Figure A 7. The full time series over the Mississippi river plumes box (Figure A 9) gives a larger dispersion, but with little consistency due to the lack of data during the C/X-band period (2002-2010) with a value of 0.5 pss than during the L-band period starting from 2010 with 0.3 pss.

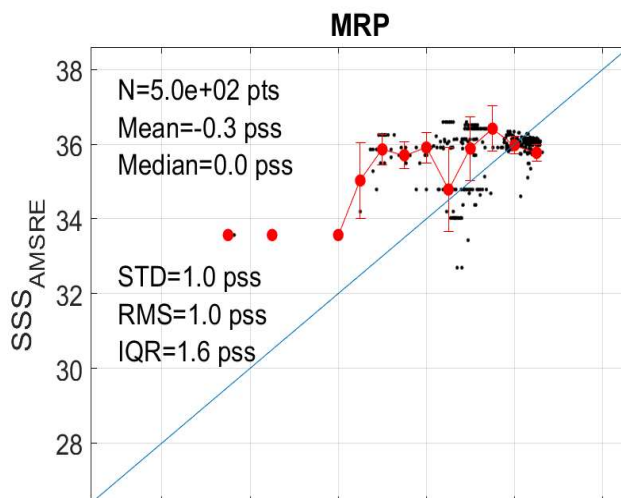


Figure A 7: Pairwise comparison between CCI C/X-band and in situ measurements from (left) EN4 and (right) CORA datasets

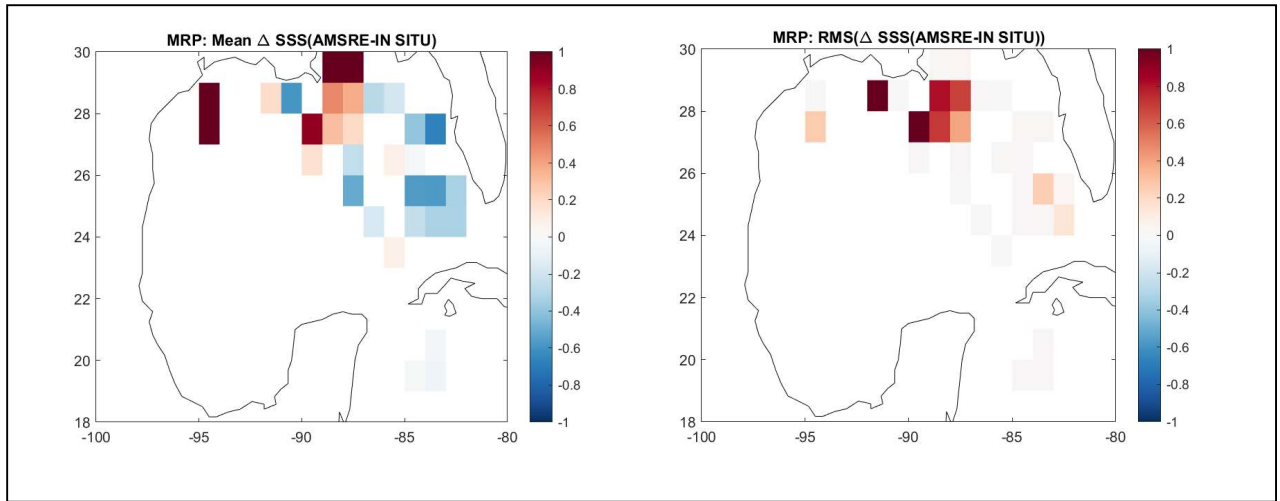


Figure A 8: Pairwise comparison between CCI C/X-band and in situ measurements on a 1°x1° grid and showing (left) the mean difference and (right) the RMSD.

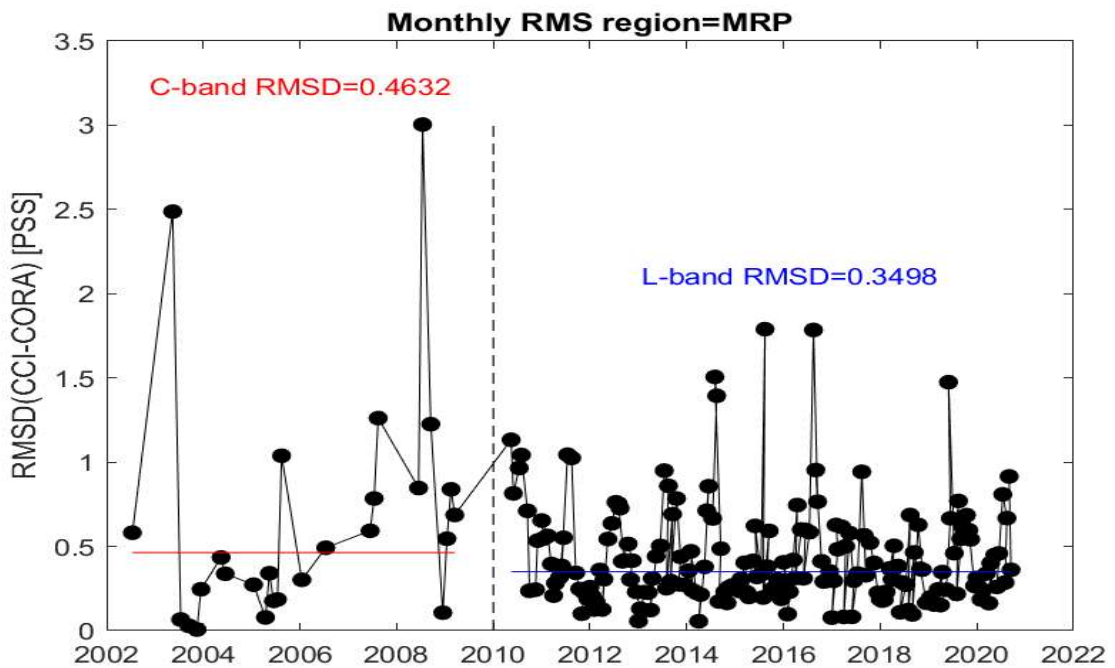


Figure A 9: Time series of the RMSD against EN4 over the Bay of Bengal for the full time series including the C/X-band and L-band period.

A4. Bay of Bengal

Comparison of CCI C/X-band dataset against EN4 in the Bay of Bengal for the 2002-2011 period (21,000 pairs) gives an overall positive mean bias of 0.2 pss (0.3 pss for the median) with a dispersion of 0.7 pss (RMSD of 0.7 pss). The CCI C/X-band dataset (black line in Figure A 10) as a lower dynamic to SSS resulting in positive biases against in situ (here EN4 and CORA) at low salinity and negative bias at high salinity. The spatial bias and dispersion in Figure A 11 follow the main position of the river plume flowing from the North to the South-East. The positive bias over this fresh salinity area is consistent with results from Figure A 10. The full time series over the Bay of Bengal (Figure A 12) gives a dispersion about twice as big during the C/X-band period (2002-2010) with a value of 0.7 pss than during the L-band period starting from 2010 with 0.3 pss.

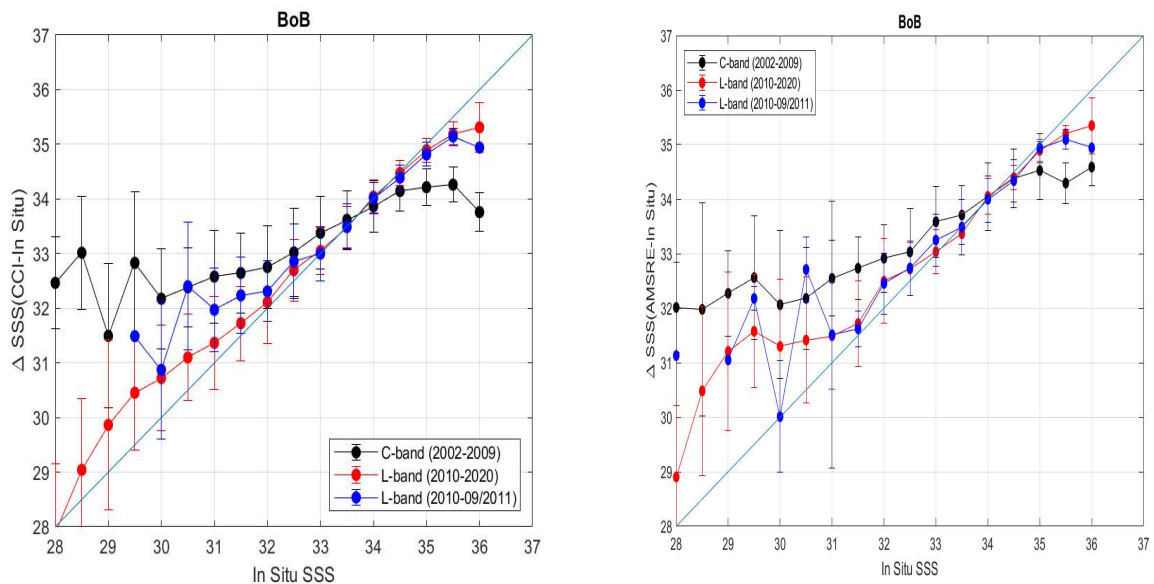


Figure A 10: Pairwise comparison between CCI C/X-band and in situ measurements from (left) EN4 and (right) CORA datasets

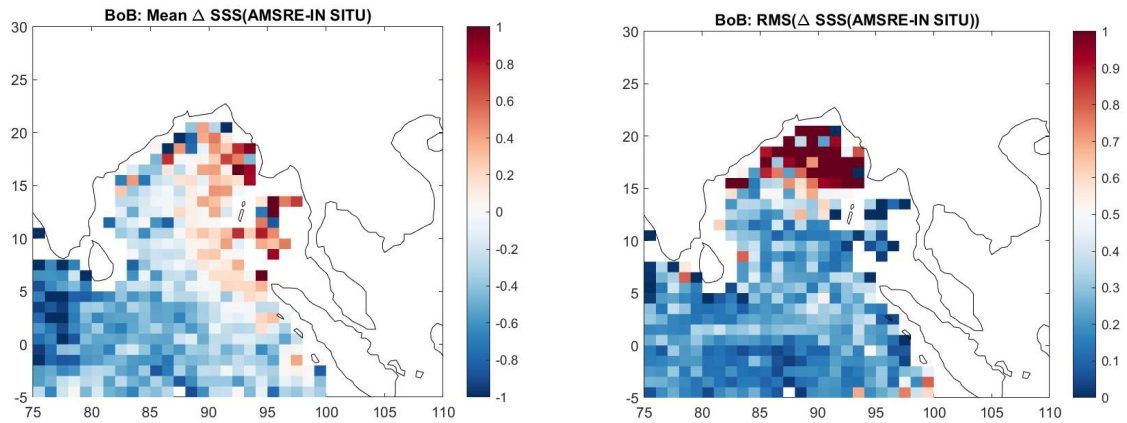


Figure A 11: Pairwise comparison between CCI C/X-band and in situ measurements on a $1^\circ \times 1^\circ$ grid and showing (left) the mean difference and (right) the RMSD.

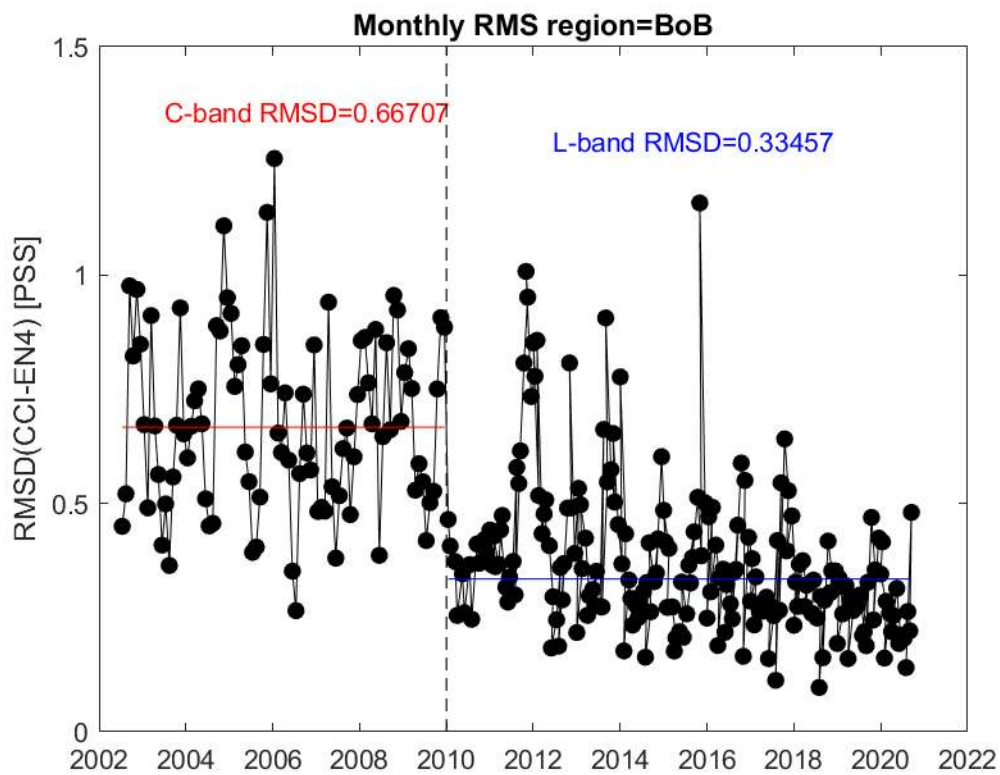


Figure A 12: Time series of the RMSD against EN4 over the Bay of Bengal for the full time series including the C/X-band and L-band period.

End of document